TÉCNICO LISBOA

MODELLING OF A MICROGRID IN A PUBLIC BUILDING

Andy Nicolas Lerens

Thesis to obtain the Master of Science Degree in

Mechanical Engineering

Supervisor: Prof. Carlos Augusto Santos Silva

Examination Committee

Chairperson: Prof. Edgar Caetano Fernandes
Supervisor: Prof. Carlos Augusto Santos Silva
Member of the Committee: Dr. Rui Pedro da Costa Neto

January 2021

ACKNOWLEDGEMENTS

I wish to thank my parents, brother, and sister for the endless support, allowing me to follow my own path and proving that no distance can ever severe our bonds. I wish to thank my grandparents for housing me and always taking care of me. I wish to thank my partner for the companionship, understanding and love. I wish to thank my soon to be born daughter for helping me look forward and be hopeful for the future.

ABSTRACT

The need to create sustainable, efficient, and affordable energy is changing the way power systems operate and innovative solutions are being developed. Microgrids are one of these solutions and the work the conducted for this thesis serves towards the integration of this technology for the creation or retrofit of Near Zero Energy Buildings. The photovoltaic, energy storage system and inverters of an existing microgrid are modelled in Simulink, allowing for the evaluation of the viability and performance for the integration of this type of renewable energy resources but also to understand the interfacing elements between the generation and the load.

Keywords: energy; microgrid; sustainable; Renewable; Energy Storage System; Simulink; performance; photovoltaic.

RESUMO

A necessidade de criar energia sustentável, eficiente e barata está a mudar a maneira como os sistemas de distribuição energética operam e soluções inovadoras estão a ser desenvolvidas. Micro redes são uma destas soluções, o trabalho desenvolvido nesta tese está direcionado para a integração deste tipo de tecnologia na adaptação de edifícios existentes em Edifícios de Consumo Energético Quase Nulo. O sistema fotovoltaico e sistema de armazenamento de energia de uma micro rede existente é modelada em Simulink, para obter uma avaliação da viabilidade e performance da integração deste tipo de fontes de energia renováveis, mas, também compreender os elementos que se encontram entre a fonte de energia e a carga do sistema.

Palavra-chave: energia; micro rede; sustentável; renováveis; armazenamento de anergia; Simulink; fotovoltaico.

TABLE OF CONTENTS

LIST OF TABLES

LIST OF FIGURES

LIST OF ABBREVIATIONS

AC – Alternating Current

ASAI – Average Source Availability Index

CERTS – Consortium for Electric Reliability Technology Solutions

DC – Direct Current

DER – Distributed Energy Resource

DG – Distributed Generation

ENS – Energy Not Serviced

ENS – Energy Not Supplied

ESS - Energy Storage Systems

ETS - Emission Trading Scheme

GHG - Greenhouse Gas

IEA - International Energy Agency

LNEG – Laboratório Nacional de Energia e Geologia

MPPT – Maximum Power Point Tracking

NZEB – Near Zero Energy Building

PCC – Point of Common Coupling

PMSG – Permanent Magnet Synchronous Generator

PNEC – Plano Nacional Energia e Clima

PQ – Power Quality

PV - Photovoltaic

PWM – Pulse Width Modulation

Comentado [RCN1]: Alphabetical order

RES – Renewable Energy Source

SAIDI – System Average Interruption Duration Index

T&D – Transmission and Distribution

THD – Total Harmonic Distortion

VUF – Voltage Unbalance Factor

WECS – Wind Energy Conversion System

1 INTRODUCTION

1.1 Motivation

Energy is one of the principal pillars that sustain our economic and social development, and its importance is relevant at all scales. From the statistics available in the International Energy Agency (IEA), the share of energy consumed in the transportation of goods and people in Portugal, represented 35% of the total final consumption in 2017, 28% for the industry, and 27% for residential, commercial and public services. The mentioned shares, and their evolutions throughout the years can be inspected in the figure 1, from a data set from 1990 to 2018.

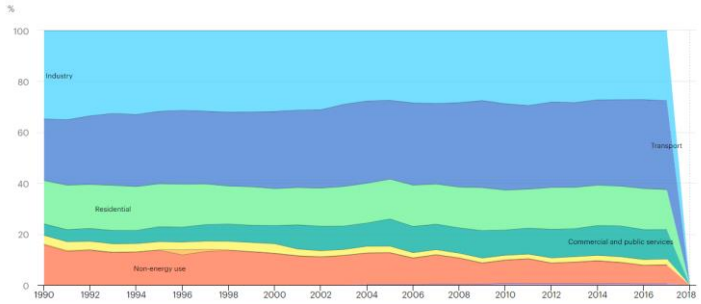

Figure 1 - Total final consumption (TFC) by sector, Portugal 1990-2018 (IEA) [1]

From further observation of the data provided by the IEA, pictured in the Figure 2 is the electricity consumption in Portugal between the periods of 1990 and 2018. The general trend is an overall increase in the electricity final consumption. In the spawn of 28 years the electricity consumption in Portugal roughly doubled, from 25 TWh to approximately 52 TWh in 2018. The 12 years prior to 2018 do not exhibit a large increase, this result can be hypothetically explained by a concoction of various factors such as, improvements in efficiency in electrical equipment, the economic crisis that struck the country in 2008 and increase in electricity prices. In [2] is illustrated the relation between the GDP and the electricity demand in China, the period of the financial crisis is highlighted by a reduction in the GDP and deep in electricity demand. An analogic standpoint can be made in Portugal where some industries such as construction and tourism were hit strongly.

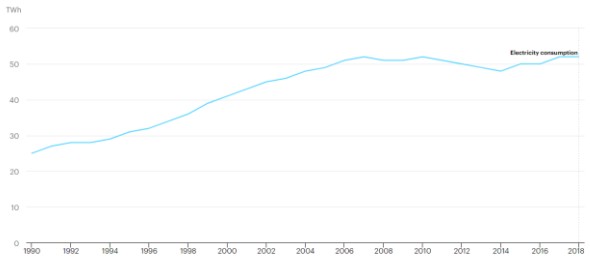

Figure 2 - Electricity final consumption, Portugal 1990-2018 (IEA) [1]

On the other hand, policies to reduce the carbon emissions, are driving the push for the integration and development of renewable energies to power the national grid, averting the use of fossil fuels plants and more carbon intensive alternatives. The prime minister of Portugal, António Costa, in 2016 said "Portugal reafirma o seu firme compromisso de ser neutro em emissões de GEE até ao final da primeira metade do século". Meaning that Portugal will work toward the goals, established in the Paris Agreement, for the energy and climate in Europe for 2050. The guidelines and goals [3] established by the protocol consists in:

- Give priority to Energy Efficiency;
- UE to become world leader in Renewable Energy;
- Equitable conditions for consumers;
- Carbon neutrality of economies;
- Promote carbon dioxide absorbers;
- Reduction of carbon dioxide emission from Emission Trading Schemes (ETS) and non-ETS sectors.

In Table 1, extracted from the National Plan for Energy and Climate 2030 (PNEC 2030), are described the tangible results obtained in Portugal and future objectives for energy and climate in Europe.

Table 1 - Portugal Results and Goals for Energy and Climate [3]

	Results from 2016	Objectives for 2020	Objectives for 2030
Greenhouse Gas Emissions[1]	8%	-18% to -23%	-45% to – 55%
Energy Efficiency[2]	23%	25%	35%
Share of Renewables	28,5%	31%	47%
Renewables in Transportation	7,5%	10%	20%
Power Grid Interconnection	8%	10%	15%

It is in this matter that microgrids can contribute to improving and acting upon the power grid interconnection and the inclusion of a bigger share of renewable energies in the power grid. Microgrids are the combination of various micro sources with rated power typically inferior to 100 kW and their interaction with the local load (power and heat). Microgrids operate connected with the conventional national power grid (supply and consumption) but can also function disconnected from the grid in islanded mode, autonomously. Generally, the Distributed Generation (DG) sources integrated in the microgrids consist of Renewable Energy Sources (RES), such as micro turbines, photovoltaic panels and Fuel Cells [4].

1.2 Objectives

The objective of this thesis is to develop the knowledge, tools and models to create a simulation environment of a microgrid implemented in the Laboratório Nacional de Energia e Geologia (LNEG). The microgrid development and study is part of the project IMPROVEMENT, with the general objective to renovate and/or convert existing public buildings in near zero energy buildings (NZEB) with usage of microgrids armed with combined heat and power (CHP), RES and energy storage systems (ESS). Other objectives of the project include developing control and management systems to guarantee energy efficiency and power quality. In the work developed in this thesis,

[1] Without Land use, land-use change, and forestry in comparison with 2005 values

[2] Reduction in the Primary Energy consumption in non-energetic uses. Comparison with projections from the model PRIMES 2007

the focus is to model the photovoltaic generation of the system, loads and the power converters to quantify the power developed by the model, and estimate the performance of the microgrid with the data available for its location.

1.3 Structure of the thesis

The thesis is structured in six main chapters. In Section 2, Literature Review, will be described the state of the art regarding the integration of microgrid in the world. In section 3, Data and Methodology, the pilot plant will be characterized, and the mathematical models used to model each individual Distributed Energy Resource and its elements. In Section 4, the Matlab/Simulink models that form the microgrid are explained. In Section 5, Results and Discussion, the results are showcased, and it is confirmed if the Model works as intended and if the microgrid performance meets its expectation and needs. Section 6 is the conclusion, where an overview of the challenges experienced to develop the models, short coming and future work.

2 Literature review

2.1 State of the Art

The main features of microgrids that make them attractive include their ability to improve grid performance, be it in case of the utility grid failures or to complement existing power generation through integration of control systems, increase renewable energy penetration or energy management tools. Microgrids are small-scale power systems comprised of local DG, energy storage systems and management and control systems.

2.1.1 Classification of Microgrids

From the elements presented previously and analyzing the microgrids facilities by their responsibility and integration in perspective from the power utility, three types of microgrids can be highlighted. Facility microgrids, utility microgrids and remote microgrids. The following Table 2, taken from [5], summarizes the types of microgrids and their main features.

Facility Microgrids have the bonus of being easier to implement than the other types. The restrictions on the implementation of this microgrids are loose, there are no real issues with the required technologies to implement this type of project and usually fits within the regulatory structure. These characteristics explain why most of the well-known demonstrations of microgrids are of this type [6].

Utility microgrids, also referred as community microgrids, are also known examples of deployment of microgrids. Technically very similar to facility grids but differ in terms of regulation and business model perspective. Utility microgrids must comply tightly with the existing utility codes. The mode of operation is grid tied, the corollary of this feature is to increase RES penetration and improve resiliency and reliability of the utility network.

Remote microgrids are isolated systems completely disconnected from the utility grid. This type of system is usually found in distant areas with no T&D utility networks and involves diversified types of Distributed Energy Resource (DER). Take the example of Isle of Eigg, in Scotland [7]. Prior to 2008, the residents of the 31 square kilometer Isle, had electricity generation predominantly dependent of the local's diesel generators and few private mini-hydro systems, producing and consuming electricity locally less than 5 hours a day. In 2008 the Isle launched its remote microgrid, integrating one large and two small hydro power generators, contemplating 110 kW, 24 kW from four wind turbines and 32 kW from PV generators. To complement the generators an energy management and control system were additionally dispatched to meet the energy consumption requirements of the island. In this case the remote microgrid became an island wide community microgrid.

Comentado [RCN2]: Clarify

Table 2 - Detailed Classification of Microgrid [5]

Microgrid Classification	Integrated Level	Utilities Impact	Responsibility	Application Area	Operational mode	Geographical Span	Power Quality	Remarks
Facility Microgrid	Middle Level	Little impact	For Vital Systems Complementation	Mainly found in NA specially for industry/institution application where technology is mature	Intentional or unintentional Islanded Mode	±3 km	High	Great use of RE, Reducing Pollution and GHG emission, High PQ and reliability for sensitive loads as well to business-entity
Remote Microgrid	Low Level	No impact	Independent System for Electrification	Mainly found in distant areas, islands and developing countries	Islanded Mode	±50km	Relaxed	Mostly Decentralized Control and maximum power use is limited to costumers
Utility Microgrid	High Level	Massive impact on utilities	For support of Power Systems	Mainly found in Japan, Europe, China where RE is rapidly developing	Grid Tied Mode	±25km	Medium	Providing high power quality, Reliability to sensitive local loads, contributing to utility stability and robustness

Microgrids can also be classified in function of the type of power supplied into the distribution network, AC microgrid systems and DC microgrid systems [8].

The main features of AC power that pushes its integration in microgrid and generally in power systems is the ability to effortlessly transform power into various levels of output for different applications, the majority of electronic loads operating in AC and the capability of long-distance transmission of power with few losses. AC microgrids can easily be connected to the utility grid bypassing conversion equipment and control strategies.

DC microgrids in contrast with AC microgrids, benefit from a better efficiency for transmission of power over short distances. The sources used for generation are generally environmentally friendly (solar and fuel cells) and require less effort in conversion processes. Most ESS are armed with storage elements (batteries, flywheels, ultra-capacitors) that benefit from DC power avoiding usage of costly converters. Multiple power systems benefit from the deployment of DC distribution systems, such as, spacecraft, electrical vehicles, telecommunication, traction, shipboard power systems, and experimental setups [9].

A comparison for AC and DC in microgrids is presented in Table 3, although the common practice is not to simply utilize one type of power supply on distributed generation, but use what is most beneficial according to location, demand and other factors. Then adapt the microgrid with different current buses, power converters and control strategies to guarantee power quality and that the loads are properly supplied.

Table 3 - Comparison of AC and DC microgrids [8]

FACTORS	AC	DC
CONVERSION EFFICIENCY	Multiple energy conversions reduce efficiency	Less conversion processes increase efficiency
TRANSMISSION EFFICIENCY	Continuous reactive losses reduce efficiency	Absence of reactive components increases efficiency
STABILITY	Affected by external disturbances	Free from external effect
SYNCHRONIZATION	Synchronization required	No synchronization issues
POWER SUPPLY RELIABILITY	Supply can be affected during seamless transfer	Power supply generally reliable
MICROGRID CONTROL	Control process complex due to frequency	Simple control approach
PROTECTION SYSTEM	Simple, cheap and mature protection schemes	Complex, costly and immature protection components
SUITABILITY	AC loads	DC loads
CALCULATION METHODS	Complex numbers involved	Only real numbers needed

2.1.2 Islanding

Islanded mode of operation is the ability of a microgrid to disconnect from the utility grid at the point of common coupling (PCC). The consumers load is instead shifted to the microgrid DG and Energy storage system (when present), the distribution utility loses control of the supply, ceasing to guarantee power quality and stability. There are many reasons for a microgrid to transition to islanded mode some of these are economic purposes, reliability instances and/or to supply power in remote locations where the utility-grid is insufficient.

2.1.3 Grid Performance Support

There are strong arguments and values for the research and development of microgrids. Of those, of most importance and more appealing for support to the grid performance are reliability, resilience and power quality [10].

Reliability is the characteristic of a system, machine or a test to perform a required task, on demand, without degradation or failure, maintaining performance. External conditions, such as storms, or equipment failures can provoke power outages, hence impacting the reliability of the electricity supply. Some microgrids are deployed to improve this metric, as they are armed with automation and control systems and DERs (Distributed Energy Resource) to allow a disconnection of the utility grid while maintaining power supply to essential components, through islanding. Microgrids have the inherent characteristic to use DERs to supply power. Generally located in proximity of the consumer loads, bypassing several disturbances related to the transmission and distribution network (T&D). Increased flexibility is provided as well via master controllers that adjust the loads accordingly to the demand, reducing costs related to energy not supplied (ENS).

The reliability of the supply of power can be assessed with the usage of several indices that measure the customer average interruption duration and/or frequency. A paper that studies the economics and reliability of microgrid energy management systems [11], compared the Average Service Availability Index (ASAI), System Average Interruption Frequency Index (SAIFI) and system average interruption duration index (SAIDI) for two different reliability simulations. The difference between the simulations is the inclusion of DERs. Resulting in, Table 4, better ASAI, SAIFI and SAIDI performances for the grid with DERs. The paper authors suggest that the improved performance is due to the ability of islanding of the microgrid when the main grid fails.

Comentado [RCN3]: Can you explain to me how it works the reliability of the micro grid?

Comentado [RCN4]: What is that?

Table 4 - Reliability simulation for a grid with and without DERs [11]

SYSTEM RELIABILITY INDEX	WITHOUT DER	WITH DER
SAIFI (1/YR)	0.4893	0.3954
SAIDI (HR/YR)	4.486	3.961
ASAI	0.99931	0.99959

A paper that focuses in resiliency improvement in electricity supply [12], defines resiliency as the capability of power systems to sustain power in unlikely and high impact incidents, ensuring the least amount of disruption in the supply of electricity, enabling quick recovery and restoration of the normal steady state of operation. The implied incidents can take various forms, natural disasters, cyber-security attacks, military interventions, etc. Hence the motivation for the integration of resiliency microgrids in strategic locations that are susceptible to this range of conditions.

The growing application of voltage sensitive loads and diversification in electric loads requires significant need for higher power quality (PQ). Microgrids in grid performance support systems are a fast and efficient way of regulating power quality through local control of voltage, frequency, current, load and dependent systems like ESS[10].

In [13] a PQ analysis is performed for a microgrid located in Newcastle at the CSIRO. The paper suggests a method for analyzing the behavior of the microgrid energy quality, either connected to utility grid or in islanded mode. The main PQ issues are identified as, frequency and voltage variations, unbalanced voltages, current and voltages total harmonic distortion (THD). For each of this concerns, tools and calculations methods are proposed to quantify and compare with defined standards. The experimentation is realized for both on-grid and islanded mode, and different sets of generation and loads conditions are tested, mainly to describe the intermittent nature of PV and Wind power, and the impact on the PQ of the supply. The minimum deviation and variation were found for on-grid mode, and the largest for islanded mode of operation, but well within the tolerance level of the Australian Network Standard, which the paper authors use for reference. Unbalanced voltages and neutral current levels maintained within tolerance level for all conditions. The minimum voltage unbalance factor (VUF) was found for unbalanced PV generation with no load condition, and gradually larger VUF with the unevenness of the load conditions while maintaining unbalanced PV Generation. Voltage THD levels were within the tolerance level proposed by the Australian Standards, however current THD levels were identified above the tolerance levels for a minimum power level of PV generation. Indicating the necessity for improvements and research in this regard. The purpose of the paper [14] is the same as the previous, to analyze the PQ of a microgrid, but uses PSS-Sincal, a commercial software developed by Siemens, to evaluate the VUF, voltage and frequency variations, voltage and current THD and neutral current. The paper concludes reasoning that the issues are mainly a consequence of the intermittent nature of DG sources with PE converter technology and the presence of non-linear and uneven load in the microgrid network. The paper also suggests that future research for PQ improvements may pass through the integration of ESS for PQ compensation and optimum control and strategies.

2.1.4 The CERTS microgrid

The Consortium for Electric Reliability Technology Solutions (CERTS) microgrid project is acknowledged as the most relevant microgrid in the U.S. The testbed located in Ohio, had for main objectives the research and development of technologies and techniques to facilitate the interconnection between local micro generation and the utility network and design control and protection strategies for different types of microgrids. The project ended up being successful leading to three major techniques, referred to as the CERTS Microgrid concept, reducing the need for custom field engineering for operation of microgrids equipped with micro generation. The techniques developed are a method for automatic and smooth transition between grid-tied and islanded mode of operation, electrical protection within the microgrid and voltage and frequency stability while in islanded-mode without usage of high-speed communication [15][16]. The testbed is designed to serve as powerful demonstration of the utility of the integration of DER, control strategies and to increase the visibility of this type of projects for commercial activities.

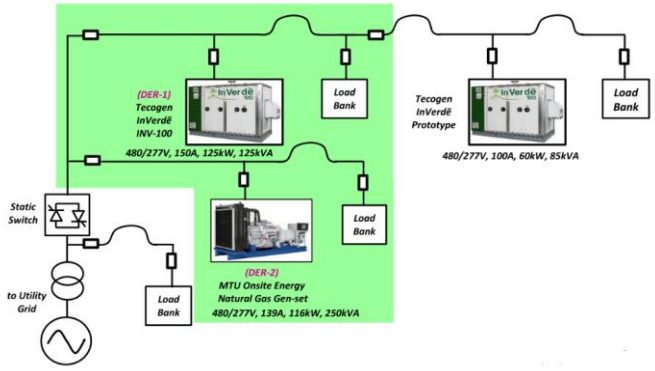

Figure 3 - Simplified schematic illustration of the CERTS microgrid natural gas generation [17]

Originally the system was comprised of three Tecogen generators (natural gas) at 480 V, with a power output of 60 kW and 60 kVAr and four load banks capable of 100 kW and 20 kVAr of consumption each. A simple schematic of the CERTS microgrid testbed is illustrated, in figure 3, indicating its distributed generators, load banks and the utility interface. The represented testbed was used for control and modelling for the gas generation, which had particular interest in the generators in the green shaded region, Tecogen INV-100 (DER-1) and a MTU Onsite Energy natural gas generator (DER-2). The testbed is again represented, figure 4, easing the identification of the three feeders in the system, the micro sources, load banks and their interconnection. Feeder A is fed by two generators (A-1 and A-2), has two load banks and uses a four-wire cable with a common ground connecting the system. Feeder B is fed by only one generator, uses a three-wire cable and has only one load bank. Both feeders A and B can transition into islanding through the static switch and support their respective load as well as the load bank in feeder C (which is then disconnected from the utility grid). The voltages and waveform in each phase are monitored through the digital data acquisition system. Some of the additional equipment's represented are shunt trip breakers and protection relays [18].

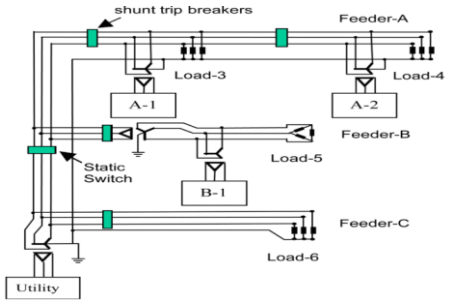

Figure 4 - CERTS microgrid testbed [18]

3 Data and Methodology

3.1 Case Study Description

The system to be analyzed is a microgrid pilot plant located in the LNEG main building. The microgrid implementation comes from the need to demonstrate technologies and strategies to convert existing buildings into NZEB (Near Zero Energy Building). To do this, the heat and electrical generation is generated from RES forming a combined heat and power (CHP) system configuration, recuperating heat from electrical sources dissipation, instead of having it being wasted.

The thermal generation and recuperation system, Figure 5, comes from two solar thermal collectors as the main source and three hybrid Photovoltaic panels (PV/T) with a heat exchanger to recuperate heat from the solar cells (design from LNEG). The base working principle of the PV/T is identical to a general PV panel except that a heat exchanger system is placed in back plate to extract heat from the solar modules to a working fluid, improving solar cell efficiency. The working fluid, in a closed loop, subsequently serves to exchange heat with a domestic hot water tank.

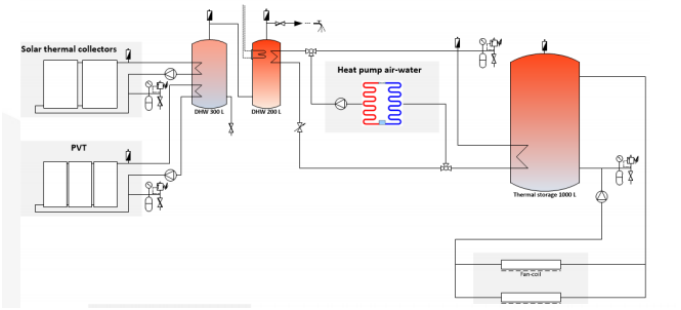

Figure 5 - LNEG's Pilot Plant thermal system

The electrical generation of the plant, Figure 6, comes from a PV array with rated power of $4{,}05\ kW$, the previously mentioned PV/T panels rated for $0{,}69\ kW$, two Training PV panels in parallel rated for $0{,}56\ kW$ and a small wind turbine rated for $2{,}5\ kW$ connected to a permanent magnet synchronous generator (PMSG). The DER output generation is in DC and is connected to a 230/400 V AC bus, interfaced individually by power electronic devices, namely inverters.

The intermittence of the RES deployed requires for added reliability hence the presence of an ESS of 48V battery with 660 Ah capacity. The main inverter interfaces the AC bus (generation), the ESS and building internal grid (loads and utility grid) and is responsible for the islanding operation of the microgrid.

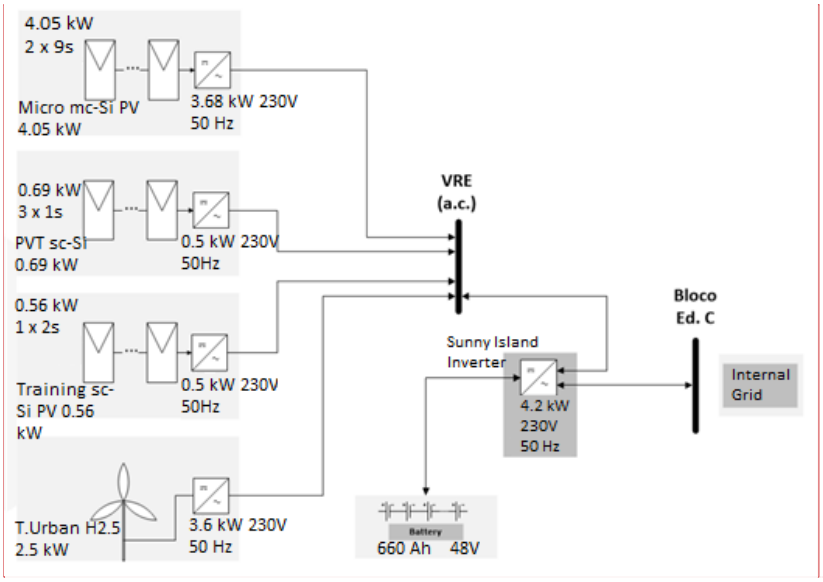

Figure 6 - LNEG's Pilot Plant Electrical System

The simulation of the microgrid presented in this thesis, will have the following assumptions and simplifications:

- The mode of operation for the simulation will be in grid-tied mode, meaning that the inverters inter-connecting the Power generation and the internal grid of the building will take the grids reference for synchronization and control;
- The loads of the microgrid are the heating pump, small appliances, and lighting, following a certain profile for the consumption;
- The loads are assumed to only require active power;
- Whenever the power generated is superior to load consumption, the battery will charge. And whenever the load is greater than the power generated the battery will discharge, to decrease the power drawn from the grid.

Comentado [RCN5]: The numbers are very small. It is difficult to read

3.2 Photovoltaic Array

3.2.1 Photovoltaic Systems

Solar irradiation is essentially one of the most abundant RES in the planet. Photovoltaic systems convert this energy source into electricity, contributing to a more sustainable environment as the operation of the system from the moment it is installed does not cause any kind of emissions and does not have any rotating parts that fail over time. The dispatch of this technology is mainly attractive in locations with a broad area and sunny weather, without any kind of shading. However due to the scalability of this type of generation its implementation is also interesting for projects smaller than vast solar plants, like rooftop integration in urban zones.

Comentado [RCN6]: How much energy is consumed por produce the PV panels?

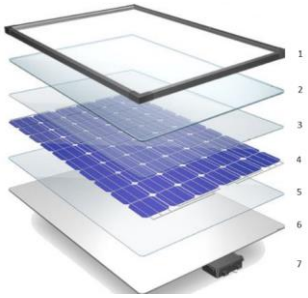

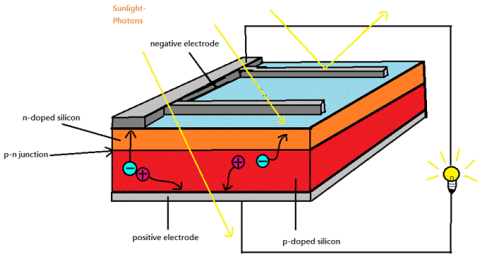

Figure 7- Solar Panel components; 1) Frame; 2) Tempered Glass; 3) Encapsulant; 4) Solar cells; 5) Encapsulant; 6) Back Sheet 7) Junction Box.

Figure 8 - PV cell working principle

PV cells are the elements responsible for the conversion of solar irradiation into electricity**,** Figure 8 represents the fundamental mechanism. The semiconductor materials are superposed, on one side the semiconductor is electrically negative and the other positive, this structure is called a p-n structure. The p-type (positive) semiconductor has the tendency to give out electrons forming holes, while the n-type (negative) intakes electrons. When Light hits the solar cell, photons excite the electrons and knocks them from the valence band into the conduction band, these electrons are now free to move. The desired direction of the flow of electrons is then supported by a conducting material connecting the bottom and top semiconductors, creating an electrical current.

For the output generation of the PV module to be useful PV cells are connected in series to generate a higher voltage and in parallel for higher current. Following the same concept, a PV array consists of PV modules firstly connected in series to attain the desired voltage and then connected in parallel to other strings to increase current and consequentially the power generation.

3.2.2 Mathematical modelling of PV Cell

The equivalent circuit of the general model of the PV Cell, Figure 9, consists of a photo current I_L, a diode, a parallel resistor to represent leakage current and a series resistor to represent the internal resistance to the current flow [19]. The voltage-current characteristic equation of a solar cell is given as

$$\boldsymbol{I = I_L - I_S\left[exp\left(\frac{q(V + IR_S)}{kT_C A}\right) - 1\right] - \frac{(V + IR_S)}{R_{SH}}} \quad (3.1)$$

Where I_S is the cell saturation of dark current, $q\ (= 1.6 \times 10^{-19}\ C)$ is the electron charge, $k\ (= 1.38 \times 10^{-23}\ J/K)$ Boltzmann's constant, T_C is the cell temperature, A is an ideal factor, R_{SH} is a shunt resistance, and R_S is the series resistance. Some models consider $R_{SH} = \infty$ and $R_S = 0$ for additional simplification, assuming there is no current leakage or current flow resistance in series. The photocurrent mainly depends on the solar insolation and cell temperature which can be expressed as

$$\boldsymbol{I_L = [I_{SC} + K_I(T_C - T_{Ref})]\lambda} \quad (3.2)$$

With I_{SC} being the cell short-circuit current at 25 °C and irradiance 1000 W/m^2, K_I being the cell short-circuit current temperature coefficient, T_C is the cell temperature, T_{Ref} is the cell reference temperature, and λ is the solar insolation in kW/m^2.

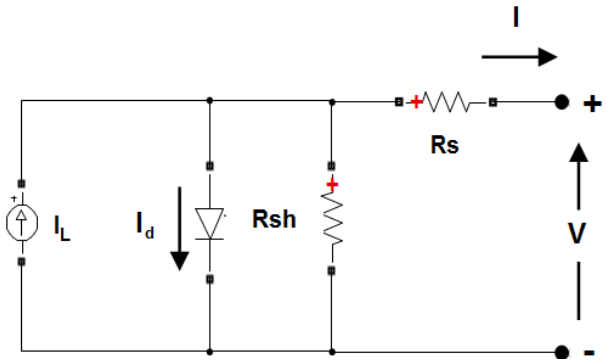

Figure 9 - Equivalent Circuit of PV Cell

Comentado [RCN7]: Not mentioned in the text

The cell saturation current, I_S, is obtained in the following way

$$\boldsymbol{I_S = I_{RS}\left(\frac{T_C}{T_{Ref}}\right)^3 \exp\left[\frac{qE_G\left(\frac{1}{T_{Ref}} - \frac{1}{T_C}\right)}{kA}\right]} \quad (3.3)$$

Where I_{RS} represents the cell reverse saturation current at a reference temperature and solar radiation, E_G is the band-gap energy of the semiconductor in the cell, A is the ideality factor which is dependent on the type of

semiconductor employed. Table 5 illustrates the value of the ideal factor depending on the type of technology employed for the PV cell.

Table 5 - Ideality factor for different PV technology

Technology	Ideality Factor A
Si-mono	1.2
Si-poly	1.3
a-Si:H	1.8
a-Si:H tandem	3.3
a-Si:H triple	5
CdTe	1.5
CIS	1.5
AsGa	1.3

3.2.3 Mathematical modelling of PV Array

The typical power generation of PV cell is roughly $2\,W$ at $0.5\,V$, requiring multiple cells connected in series-parallel to achieve a reasonable current and voltage rating. This configuration is called a PV module, the circuitry is then encased and protected in the PV panel, with a general configuration like Figure 7.A PV array is a cluster of PV modules connected in series for appropriate Voltage and in parallel to increase current. The instantaneous power of the PV array can be calculated through the electrical power law equation, with $Vpv\ (V)$ and $Ipv\ (A)$ being the PV array output Voltage and Current.

$$P = Vpv \times Ipv \tag{3.4}$$

The general equivalent circuit of the PV module is represented in Figure 10, Np being the number of cells arranged in parallel and Ns the amount of cells arranged in series.

The final equation for current and voltage of the solar array is expressed as

$$\boldsymbol{I = NpI_L - NpI_S\left[exp\left(\frac{q\left(\frac{V}{Ns}+\frac{IR_S}{Np}\right)}{kT_CA}\right)-1\right]-\frac{\left(\frac{NpV}{Ns}+IR_S\right)}{R_{SH}}} \tag{3.5}$$

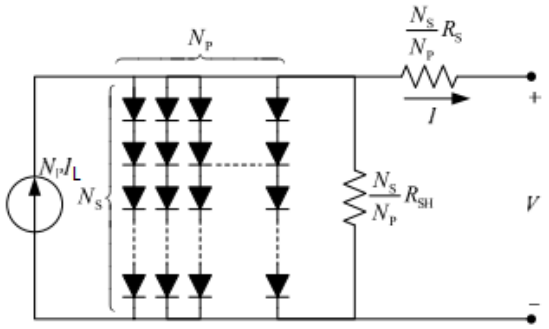

Figure 10 - General equivalent circuit of PV Array

3.2.4 Photovoltaic Panel Parameters

The Solar Panel employed in the LNEG Pilot consists of 60 (6x10) polycrystalline silicon solar cells, denominated LDK 225P-20. The electric characteristics, of the panel, in standard test conditions (STC: Irradiance of 1000 W/m^2, T=25 °C) and NOCT (Nominal Operation Cell temperature, Irradiance of 800 W/m^2, T_{air}=20 °C w=1 m/s) are displayed in **Erro! A origem da referência não foi encontrada.** and **Erro! A origem da referência não foi encontrada.**. The temperature characteristics of the module are displayed in **Erro! A origem da referência não foi encontrada.**.The temperate coefficient of the properties represent how strongly their performance relates to temperature of the cell, or the PV array surface temperature. The temperature coefficient of V_{oc} and P_{max} are negative, meaning that as the cell temperature increase the output power of the PV array decreases.

Table 6 - Electric characteristics of LDK 225P-20 module at STC

PV Module	LDK 225P-20
Nominal output (Pmax)	225 *W*
Voltage at Pmax (Vmp)	29.9 *V*
Current at Pmax (Imp)	7.35 *A*
Open Circuit Voltage (Voc)	36.7 *V*
Short Circuit Current [Isc]	8.24 *A*
Cell efficiency	15.89
Module Efficiency	13.79

Table 7 - Electric characteristics of LDK 225P-20 module at NOCT

PV Module	LDK 225P-20
Nominal output (Pmax)	163 *W*
Voltage at Pmax (Vmp)	26.7 *V*
Current at Pmax (Imp)	6.12 *A*
Open Circuit Voltage (Voc)	33.8 *V*
Short Circuit Current [Isc]	6.67 *A*

Table 8 - Temperature characteristics of LDK 225P-20 module at SDC

PV Module	LDK 225P-20
NOCT	45 +- 2 °C
Temperature Coefficient of Pmax	-0.47 % / °C

Temperature Coefficient of Voc	-0.34 % / °C
Temperature Coefficient of Isc	0.06 % / °C
Maximum Series Fuse Rating	20 *A*
Operating Temperature	-40 to 85 °C

The small 560 W PV array is composed of two 280 W rated power. The Suntech Power PLUTO280 is selected and the panel characteristics are shown in

Table 9 - Characteristics of Suntech Power PLUTO280

PV Module	Canadian Solar CS6P-230PX
Nominal output (Pmax)	280 W
Voltage at Pmax (Vmp)	36 V
Current at Pmax (Imp)	7.78 A
Open Circuit Voltage (Voc)	44.3 V
Short Circuit Current [Isc]	8.15 *A*
Temperature Coefficient of Voc	-0.304 % / °C
Temperature Coefficient of Isc	0.066 % / °C

3.3 Photovoltaic Thermal system

For the characterization of the photovoltaic Thermal (PV/T) collector used in the microgrid, very little information has been given. In this work the system will be interpreted as the fusion of the functions of a flat plate solar (thermal) collector and of a photovoltaic panel. The flat plate collector will remove the excess heat providing from the solar cells and transfer it to a working fluid. However, since the focus of the study is to determine the power generation, and not necessarily the heat transfer or the saving from pre-heating the DHW tank, the PV/T will be approximated to a simple PV Array of 1 string of 3x 230 W rated power panels. The Canadian Solar CS6P-230X is selected and the characteristics displayed in Table 10.

Table 10 - Characteristics of Canadian Solar CS6P-230X at STC

PV Module	Canadian Solar CS6P-230PX
Nominal output (Pmax)	230 W
Voltage at Pmax (Vmp)	29.8 V
Current at Pmax (Imp)	7.71 A
Open Circuit Voltage (Voc)	36.8 V
Short Circuit Current [Isc]	8.24 *A*
Temperature Coefficient of Voc	-0.347 % / °C
Temperature Coefficient of Isc	0.0359 % / °C

3.4 Wind Energy Conversion System

The wind energy conversion system (WECS) converts wind energy into mechanical energy through the use of a wind turbine, the mechanical energy is then converted into electricity through a generator. Several types of generators are employed depending in the application, such as permanent magnet synchronous generator (PMSG), squirrel-cage induction generator (SCIG), doubly fed induction generator (DFIG) and wound rotor induction generator (WRIG). Commonly, several applications of the technology employ the PMSG due to its reliability, efficiency, low cost and smaller size compared to the DGIC, SCIG and WRIG [20]. WECS can be classified by the size of the wind turbine and their axis, horizontal or vertical wind turbine, and small ($< 10\ kW$) and big wind turbine since the power output of the WECS increases with the swept rotor area.

Comentado [RCN8]: Explain me the differences of the several generators. Vantages disadvantages, sizes, maintenance, durability, applications e

Comentado [RCN9]: What type of wind turbines are the best for residential?

Generally, the WECS is composed of a wind turbine, a generator, a power electronic and a power electronic converter to connect to the grid or directly to a load. In the case of LNEG's pilot plant a small wind turbine outputs

the mechanical torque to a PMSG, generating electricity that enter a converter to feed the AC bus of the microgrid. Figure 11 illustrates the power generation for a WECS with a PMSG generator, converter, and the connection to load or electrical bus.

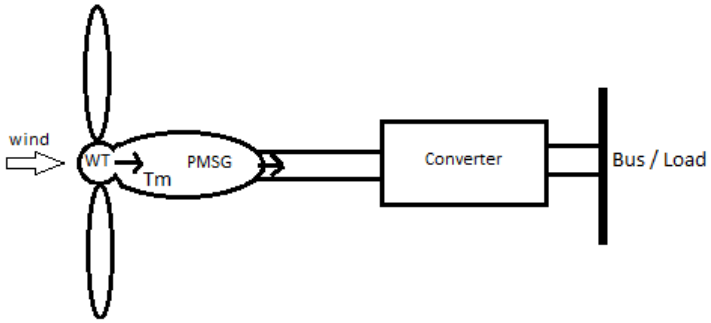

Figure 11 - WECS based on a PMSG generator

3.4.1 Modelling of the wind turbine

The mechanical power produced by the wind turbine can be expressed by [20]

$$\boldsymbol{P_w = \frac{1}{2}\rho\pi R^2 V_w^3 C_p} \tag{3.6}$$

Where C_p represents the power coefficient, the air density $\rho = 1.225\ \frac{Kg}{m^3}$, $V_w\ \left(\frac{m}{s}\right)$ is the wind speed and $R\ (m)$ is the blade radius. From the equation (3.6) it's visible that the mechanical power generated in the wind turbine is proportional to V_w^3.

The power coefficient C_p represents how efficiently the wind turbine converts the wind energy into mechanical power and can be approximated by analytic functions [21]. According to Bet'z law, based on the conservation of mass and the actuator disk theory, no turbine can convert more than 59.3% of the kinetic energy in the wind. The generic equation used to model the C_p of the modelling turbine [22] is

$$\boldsymbol{C_p\ (\lambda, \beta) = \ C_1\left(\frac{C_2}{\lambda_i} - C_3\beta - C_4\right)e^{-C_5/\lambda_i} + C_6\lambda} \tag{3.7}$$

With,

$$\boldsymbol{\frac{1}{\lambda_i} = \frac{1}{\lambda + 0,08\beta} - \frac{0,035}{\beta^3 + 1}} \tag{3.8}$$

The coefficients used in the equation (3.7) are $C_1 = 0{,}5176$, $C_2 = 116$, $C_3 = 0{,}4$, $C_4 = 5$, $C_5 = 21$ and $C_6 = 0{,}0068$. The tip speed ratio λ is expressed by

$$\boldsymbol{\lambda = \frac{\omega_w R}{V_w}} \tag{3.9}$$

Where ω_w $(\frac{rad}{s})$ is the rotor speed.

The $C_p - \lambda$ characteristics, for different values of the pitch angle β are illustrated in Figure 12. The maximum value for the power coefficient for the modeled turbine is $C_p = 0{,}48$ for the pitch angle $\beta = 0$ and$\lambda = 8.1$.

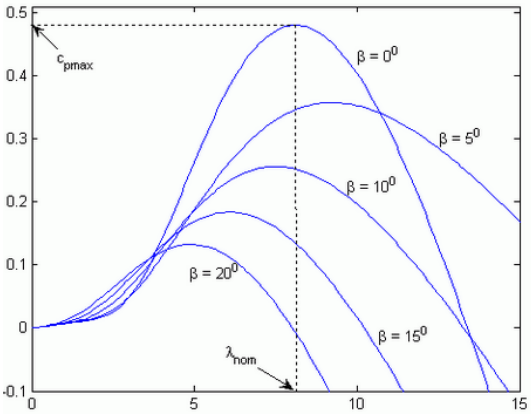

Figure 12- $C_p - \lambda$ characteristics, for different values of the pitch angle $\boldsymbol{\beta}$

Finally, the torque of the turbine T_w $(N.m)$ is given by the equation

$$\boldsymbol{T_w = \frac{1}{2}\rho\pi R^3 V_w^2 C_q} \tag{3.10}$$

With the torque coefficient being, C_q:

$$\boldsymbol{C_q = \frac{C_p}{\lambda}} \tag{3.11}$$

3.4.2 Modelling of the PMSG generator

A Permanent Magnet synchronous generator, unlike other synchronous machines replaces the DC circuit for permanent magnets, thus eliminating the brushes. The term synchronous refers to the property that the rotor and the magnetic field rotate with the same speed, since the magnetic field is generated through a shaft mounted permanent magnet mechanism, inducing the current into the stationary armature. This way, attaining a smaller size, lower moment of Inertia, meaning better reliability and power density. The rotor circuit benefits from eliminated electrical losses due to the permanent magnets. Those are the main driving reasons for implementations of this type of generators in hydro and wind turbines of smaller scale. The mathematical models presented to describe the working principle of the PMSG are based on the studies [20] [23][24].

The Electromagnetic torque generated by the PMSG generator is expressed by

$$\boldsymbol{T_e = \frac{3P}{2}(\lambda_r i_{qs} - (L_d - L_q) i_{ds} i_{qs})} \quad (3.12)$$

Where, L_d and L_q (H) are the dq-axis self-inductance of the synchronous generator, λ_r $(Wb(rms))$ is the rotor flux linkages and P is the number of pole pairs. i_{ds} and i_{qs} are the dq-axis stator current of the PMSG and are expressed as

$$\boldsymbol{\frac{di_{ds}}{dt} = -\frac{R_s}{L_d} i_{ds} + \frac{L_q}{L_d} \omega_r i_{qs} - \frac{1}{L_d} v_{ds}} \quad (3.13a)$$

$$\boldsymbol{\frac{di_{qs}}{dt} = -\frac{R_s}{L_q} i_{qs} + \frac{L_d}{L_q} \omega_r i_{ds} - \frac{1}{L_q}(\omega_r \lambda_r + v_{qs})} \quad (3.13b)$$

With R_s being the stator winding resistance, v_{ds} and v_{qs} the dq-axis stator voltage and ω_r $(\frac{rad}{s})$ the rotor speed.

$$\boldsymbol{v_{ds} = -R_s i_{ds} + L_q \omega_r i_{qs} - L_d \frac{di_{ds}}{dt}} \quad (3.14a)$$

$$\boldsymbol{v_{qs} = -R_s i_{qs} - L_d \omega_r i_{ds} + \omega_r \lambda_r - L_q \frac{di_{qs}}{dt}} \quad (3.14b)$$

The rotor speed can be described by the equation

$$\boldsymbol{\omega_r = \frac{P}{J}(T_w - T_e)} \quad (3.15)$$

J is the moment of inertia of the rotor**.**

3.5 Energy Storage System

An Energy Storage System (ESS) adds an increased reliability and flexibility to the power system, storing excess power generated from the RES when the load profile allows and powering the microgrid when DER are not sufficient to keep up due the intermittency of the generators. ESS allow for electricity to be transformed into another form, be stored, and be deployed when necessary. The energy storable in a battery, the battery capacity, can be measured either as watt-hour *Wh* (usually in the order of *kWh) or in* Ampere-hour *Ah.* For battery systems the *Ah* unit is more frequent, it determines the number of hours for which the battery can deliver a current equal to the discharge rate when the battery voltage is nominal. Nonetheless, the *Wh* of the battery can be estimated by the product of the *Ah* capacity with the nominal voltage battery voltage.

The Battery type used in the microgrid is of the Lithium-Ion (Li-Ion) type. One of the advantages of using a Li-Ion type of battery, is that the cells that form the battery operate at a voltage three times higher than usual NiMH or NiCd batteries, at 3.7 V. For this reason, Li-Ion batteries present a higher energy density (*Wh/Kg*). The increased energy density translates into a reduced amount of required battery cells for specific operations.

The main components of the battery cells are a positive and negative electrode, an electrolyte and a separator. The electrolyte is an ionic conductor providing the means for the ionic charge between the positive and negative electrodes, the separator serves as a barrier between the electrodes isolating them, it serves as ionic conductor but electrical insulator, preventing internal short circuiting which would cause the cell to self-discharge. The Li-

Ion charge and discharge principle, unlike other electrochemical cells, does not rely on redox reactions that chemically alter the reacting species at the surface of the electrodes. Instead during discharge, as represented in Figure 13, lithium atoms at the surface of the negative electrode provide electrons which pass through the external circuit and become positive ions Li^+. The Li^+ exit the electrode and dissolve into the electrolyte and move towards the positive electrode where they receive electrons from the external circuit and become neutrally charged, in the crystalline structure of the electrode. These events are reversible and switch between charge and discharge, with the Lithium ions moving back and forth between the electrodes [25].

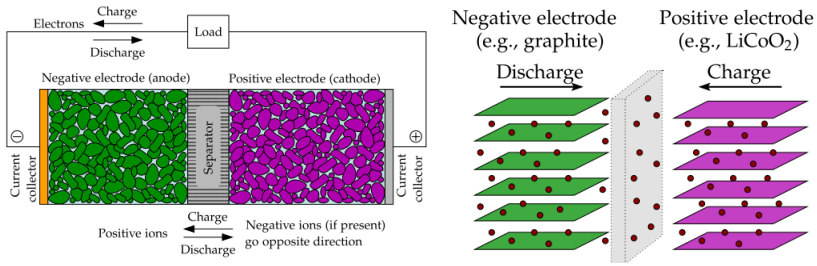

Figure 13 - Schematic diagram of lithium-ion cell [25]

Comentado [RCN10]: Not mentioned in text

The typical discharge characteristics of a battery can be found in Figure 14, the three sections of the curve are outlined. The exponential voltage drops when the battery starts discharging after being fully charged, is represented in the first section, the width of the zone is strongly related to the type of battery used. The following section, and the widest is the charge that can be extracted from the battery until the voltage drops below the nominal voltage of the battery. After the voltage drops below the nominal value, it starts to drop rapidly until no more power is extractable, the third section represent this phenomenon.

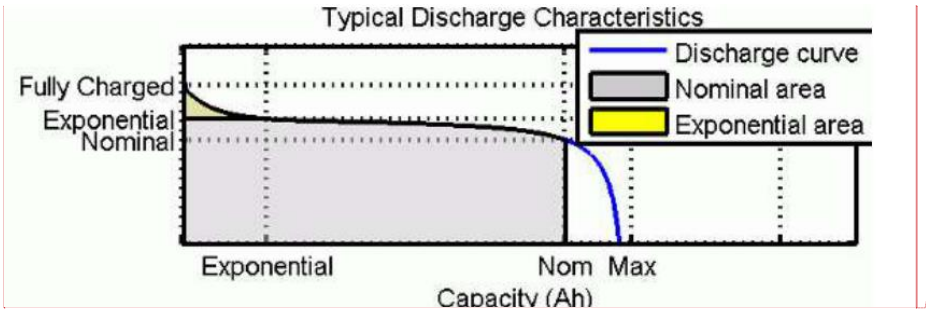

Comentado [RCN11]: The figure is cut

Figure 14 - Typical Discharge Characteristic of a Battery

When the current applied to the terminal of the battery is negative, current flows in the opposite direction, and the battery starts charging, Figure 15 represents the plotted voltage versus State of Charge (SOC) in percent of a Li-Ion and lead acid battery.

Comentado [RCN12]: What have you learned with this knowledge ?

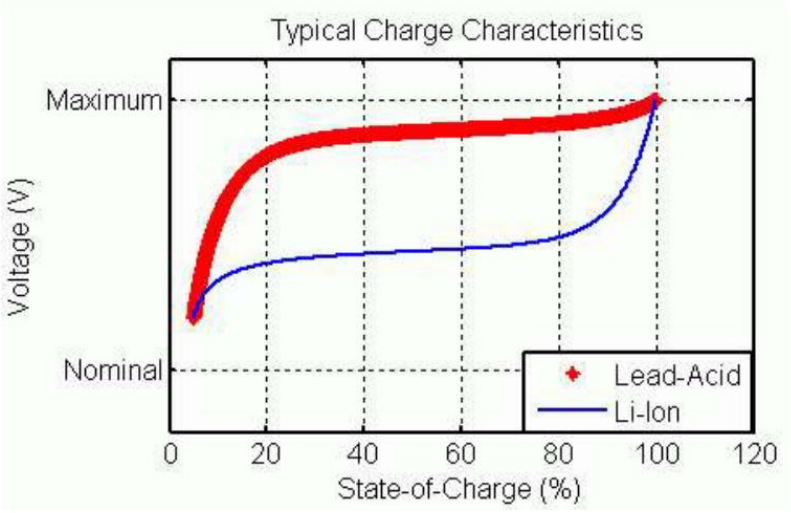

Figure 15 - Typical Charge characteristics of Lead-Acid and Li-Ion batteries.

3.5.1 Battery Model

The model of the battery used for the simulation is based on the Simscape Power Systems Library battery, the battery block implements a generic dynamic model that represents most commonly found types of rechargeable batteries [26]. Figure 16 represents the equivalent circuit of the dynamic model for the battery. The Battery type used in the microgrid is of the Lithium-Ion (Li-Ion) type.

Comentado [RCN13]: Explain me this into detail

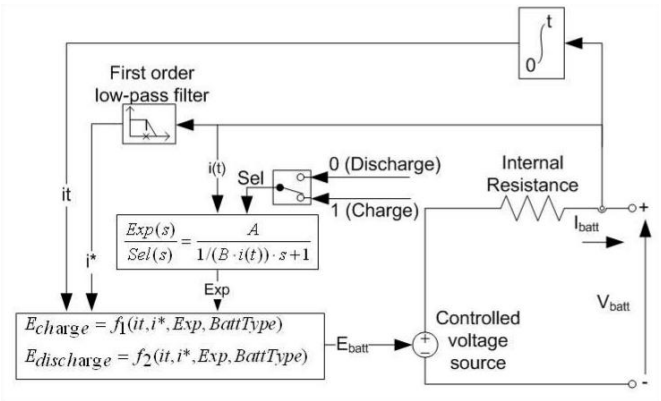

Figure 16 - Equivalent Circuit of Battery dynamic model block from [26]**.**

The parameters and variables of the model are:

- E_{batt} Nonlinear Voltage (V)
- E_0 Constant Voltage (V)
- Exp(s) Exponential Zone Dynamics (V)
- Sel(s) Battery mode, 0 for discharge 1 for charge
- K Polarization constant (Ah^{-1}) or Polarization resistance (Ω)
- i* Low frequency current dynamics (A)
- i Battery Current (A)
- it Extracted Capacity (Ah)
- Q Maximum Battery Capacity (Ah)
- A Exponential Voltage (V)
- B Exponential Capacity (Ah^{-1})

For the Li-Ion Battery type, the discharge model ($i^* > 0$) is

$$f_1(it, i, i^*) = E_0 - K.\frac{Q}{Q - it}.i^* - K.\frac{Q}{Q - it}.it + A.exp(-B.it) \quad (3.16)$$

And the charge model ($i^* > 0$) is

$$f_2(it, i, i^*) = E_0 - K.\frac{Q}{it - 0.1.Q}.i^* - K.\frac{Q}{Q - it}.it - A.exp(-B.it) \quad (3.17)$$

3.6 Power converters

The quality of the power fed to the system is required to be within certain parameters. Whether it is a certain voltage, frequency, in phase, AC or DC. To guarantee this, power converters are a widely used solution. In the case of this study, the power fed to the microgrid is required to be three-phase 230V AC.

As seen previously, the output of the solar array is in DC, which implies imperatively a converter to turn it into DC, however a transformer-less inverter requires a certain voltage input to generate the output voltage necessary for the specific application. Hence, the need to boost the DC voltage at the input of the inverter. This boosting of the DC voltage is done through a type of converter named boost converter or step up converter, which as the name implies, step ups an initial voltage to a higher level. This is particularly helpful in cases where the DC voltage of the input at the inverter is insufficient to generate adequate AC voltages. In Section 4, where the properties of the Solar Array and V-I curves are presented, a boost converter can be useful to feed the higher voltage at the input of the inverter to be sufficient to ensure that the voltage fed to grid by the inverter is 230V AC. In parallel, boost converters can be designed to extract the maximum voltage and current of the generation, making it operate at its maximum power point (MPP), through Maximum Power Point Tracking (MPPT) algorithms. Buck Converters, similarly to boost converters, take the initial DC voltage but reduce it to a lower level being useful to feed lower voltage devices like batteries. Buck-Boost converters end being the amalgam of the above-mentioned converters, being able to reduce or increase an incoming voltage, and when designed such as to operate bi-directionally. For example, in the case of a battery charging, it can take a larger DC voltage and convert it into an appropriate voltage (buck) for the battery (12V ,24V,48 V, etc.), when the dynamic of the system changes and the battery is required to feed a load or grid, the converter (boost) switches mode and increases the input voltage to the required output.

3.6.1 Boost Converter

Boost converters are used to step an input voltage to a higher output voltage. In Figure 17 the equivalent circuit a boost converter connected to the DC-link capacitor of a voltage source is illustrated. In this type of circuit, whilst the switching device is closed, the inductor current rises and energy is stored in the inductor. When the switch is opened, the energy stored in the inductor flows and is transferred through the diode and the inductor current falls [27]. The capacitor C is large enough that it can serve as buffer for the circuit, minimizing the ripple on the output voltage thus remaining approximately continuous.

The output voltage can be stepped up by varying the duty cycle D and the minimum output voltage is obtained with forcing $D = 0$, as the following equation shows,

$$\boldsymbol{D = 1 - \frac{V_{in(min)}}{V_{out}}} \tag{3.18}$$

Where $V_{in(min)}$ is the minimum input voltage and V_{out} is the desired voltage output.

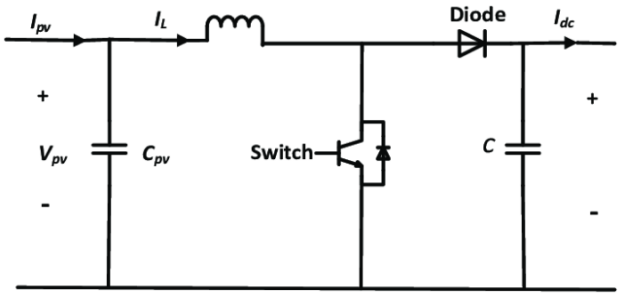

Figure 17 - Equivalent Circuit of a Boost Converter connected to Photovoltaic Source

The calculation of the components and parameters of the circuit is done through [28] calculation sheet.

An estimation for the inductor can be done through the equation,

$$L = \frac{V_{in}(V_{out} - V_{in})}{f_{sw}\Delta I_L V_{out}} \tag{3.19}$$

Where ΔI_L is the inductor ripple current, f_{sw} the switching frequency of the switch device and V_{in} the typical input voltage. The inductor value is inversely proportional to the maximum output current. This effect is also observed in the equation for the calculation of the ripple current.

$$\Delta I_L = \frac{V_{in(min)}D}{f_{sw}L} \tag{3.20}$$

In this case since the objective is to calculate the parameters for the equivalent circuit the equation 3.18 is not used. Instead the inductor ripple current is estimated being 10% to 20% of the maximum output current $I_{out(max)}$.

$$\Delta I_L = (0.1\ to\ 0.2)\ \frac{V_{out}}{V_{in}} I_{out(max)} \tag{3.21}$$

$I_{out(max)}$ can be estimated by knowing the rated power of the source P_{rated} and $V_{in(min)}$. Equation 3.20 is good enough for the estimation of the parameters in this work. For example, a PV array, voltage and current varies dependently of irradiation. Observing the V-I curves of the PV array, it's possible to estimate the minimum voltage at lower levels of irradiation whilst P_{rated} doesn't vary with operation, since it's evaluated at STC.

$$I_{out(max)} = \frac{P_{rated}}{V_{in(min)}} \tag{3.22}$$

The following equation can be used to adjust the output capacitor value for a desired output voltage ripple ΔV_{out}. Appropriate values vary from 1 to 5% depending on the electrical regulation.

$$C_{out(min)} = \frac{I_{out(max)} D}{\Delta V_{out} f_s} \tag{3.23}$$

3.6.2 Inverter

The theory to understand Inverters can be extensive, the aim of this section is not to display all the concepts behind their functioning, but to allow the reader to follow the train of thought used for the designing of the inverter for this study and more importantly the control methodology applied to it.

Inverters are a type of converter employed to convert DC input voltage to an AC output voltage of desired magnitude and frequency [27]. An inverter allows the control of the output, depending on the operation, it can be designed to output a fixed or variable voltage at fixed or variable frequency. By varying the input DC voltage and maintaining the gain of the inverter constant, a variable output voltage can be obtained, in the case of fixed DC input voltage by varying the gain of the inverter a variable output voltage can be obtained. Of the many techniques of control to vary the gain inverter, a commonly well studied one is the pulse width modulation (PWM). PWM is the technique used for this study. In ideal inverters the output voltage waveforms should be sinusoidal, but in practice the waveform contains certain harmonics and are non-sinusoidal. The output waveform is largely dependent of the type signal waveform injected in the inverter. This type of waves can be square-wave, modified sinewave, or sinusoidal waveforms, illustrated in Figure 18. Depending on the type of application the waveforms are chosen, being sinusoidal waveforms preferred for high-power applications. The harmonic contents of the output voltage and current can be reduced by the application of switching techniques and using filters such as L, LC or LCL filters. The filters and their dimensioning will be explained later in Section 4 of the thesis, along the Matlab/Simulink Models of the components of the Microgrid.

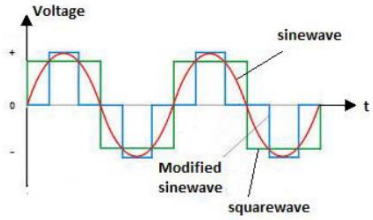

Figure 18 - Types of generated inverter waveform, taken from [29]

Comentado [RCN14]: Not mentioned in text

Comentado [RCN15]: Explain me how it works an inverter?

3.6.3 Buck-Boost Converter

Buck-Boost converter are DC-DC type of converters able to output voltages larger or lesser than the input voltage magnitude.

An equivalent circuit of a bi-directional Buck/Boost converter is shown in Figure 19, since it is of particular interest as it will be used for the ESS.

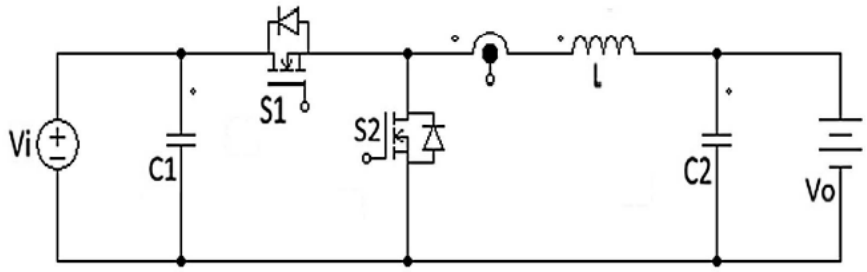

Figure 19 - Equivalent Circuit of Buck/Boost Converter [30]

Depending on the mode of operation the switch 1 (S1) and the switch 2 (S2) may be working as diode or switching device. When in boost mode S1 = 0 thus serving as a diode, S2 switching is responsible for stepping the voltage Vo to Vi. In Buck mode, S2 serves as the diode and S1 switching is responsible to reduce the Vi voltage to a lower Vo.

The critical values for inductor L_c and capacitor C_c can be calculated resorting to Equation , demonstrated in [31]. D is the large signal duty cycle, f_{sw} is the switching frequency and R is the load resistance.

$$L_c = \frac{D(1-D)}{2fsw}R \tag{3.24}$$

$$C_c = \frac{D}{2fswR} \tag{3.25}$$

4 Matlab and Simulink Integration

4.1 Photovoltaic Array Model

Simscape Electrical is a toolbox integrated in Simulink providing component libraries for modeling and simulating electronic, mechatronic, and power systems. The modelling of the PV array of the LNEG Pilot plant, is implemented with the block PV Array. The array is built of strings of modules connected in parallel with each string consisting of modules connected in series. A vast library of modules from the National Renewable Energy Laboratory (NREL) are available and each module parameters can be defined by the user.

The PV array block consists of a five parameter model using a light generated current (I_L), diode (saturation current I_0 and ideality factor n_l) series resistance R_s, and shunt resistance R_{sh} to represent losses related to irradiance and temperature dependent I-V characteristics of the modules.

From the PV module properties of PV panel presented in Section 3.2.4, and inserting them on the module data window, Figure 20, of the PV array block, the five parameters of the model are obtained. $I_L = 8.2856$ A, $I_0 = 1.3372 \times 10^{-10}$ A, the diode ideality factor $A = 0.9612$, $R_{sh} = 56.8142\ \Omega$ and $R_s = 0.31408\ \Omega$.

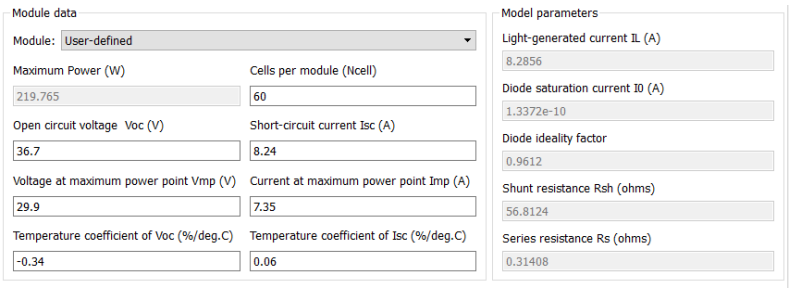

Figure 20- Model Parameters obtained from PV array block in Simulink

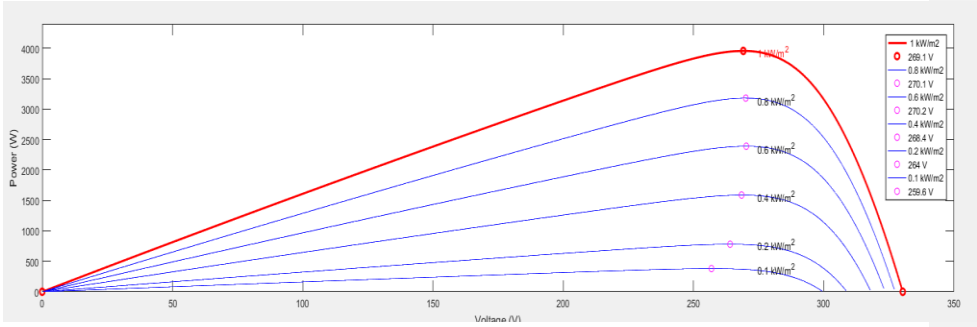

Figure 21 - Power - Voltage curve of the 4 kW modeled PV array

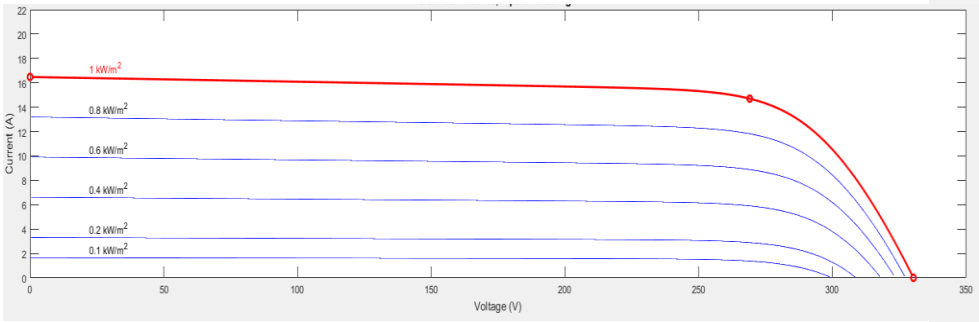

Figure 22 Current - Voltage Curve of the 4 kW modeled PV Array

Figure 21 and Figure 22 are, respectively, the obtained P-V and V-I curves for the 4 kW PV Array of the Microgrid, at different values of Irradiance and at 25 °C. The curves reflect the important impact of the irradiance in the power generation of the source, and how important it is to control the behavior of the current and voltage such that maximum efficiency is achieved, thus generating the most power available. For instance, at 1000 W/m^2 the maximum power can be extracted with the PV array operating at 269.1 V and 14.7 A generating the rated 4 kW power.

Many studies that investigate the PV array modelling use the ambient temperature to represent the cell temperature, however this assumption is not representative of every situation, the study [32] calculates the cell temperature, with the Equation 4.1 , as a function of the air temperature and irradiance variation.

$$T_{Cell} = 1.14(T - T_{STC}) + 0.0175(G - 300) + 30 \quad (4.1)$$

Comentado [RCN16]: Do the legend explain the parameter of the equation after.

Where T is the air temperature in °C, T_{STC} is the standard test condition temperature of 25 °C and G is the solar irradiation in W/m^2.

4.1.1 Grid-Connected PV Array

Each generator of the microgrid is modeled and simulated separately before the microgrid assembly, to ensure that the models are robust enough to obtain useful results for the evaluation of the performance of the system. The model of the 4 kW PV array, along with the two-stage inverter is presented in Figure 23. The PV Array input is the global irradiance (Ir) over the surface of the panel and the temperature of the cell (Tcell), the PV Array terminals are connected to a DC/DC boost converter to step up the voltage of the array to constant 600 V, whilst maintaining optimum generation. The boost converter is then connected to the DC/AC Inverter converting the 600 V DC to the 230/400 V (phase to ground/phase to phase) AC Bus and Grid. The LCL filter is used to reduce the harmonics and flickers generated by the converters, for smoother sinusoidal waves at the output.

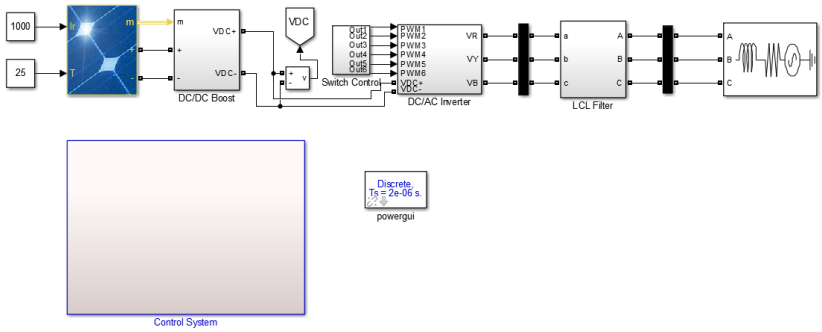

Figure 23 - Grid connected modeled PV Array

The LCL filter calculations in this thesis are done following the procedure demonstrated in [33].

The base capacitance C_b is calculated by the equation

$$C_b = \frac{1}{\omega_g Z_b} \tag{4.2}$$

With $\omega_g = 2\pi f$ being the grind angular velocity and Z_b being the base impedance is calculated by

$$Z_b = \frac{E_n^2}{P} \tag{4.3}$$

The inverter side inductance L_1 can be calculated using equation

$$L_1 = \frac{V_{DC}}{6 f_{sw} \Delta I_L max} \tag{4.4}$$

Where V_{DC} is the DC link voltage, f_{sw} is the switching frequency of the inverter and $\Delta I_L max$ is the maximum allow value for the current to fluctuate as is rated at 10% of the maximum current through the filter. The capacitor value is then calculated by

$$C_f = 0.05 C_b \tag{4.5}$$

The grid side inductance L_2 is calculated by

$$L_2 = \frac{\sqrt{\frac{1}{k_a^2} + 1}}{C_f \omega_{sw}^2} \tag{4.6}$$

Using k_a = 0.2 as the attenuation factor.

The LCL filter values, for each individual line, used for the simulation is presented in Table 11.

Table 11 – Inductor and Capacitor values selected for each individual line

Branch	L1	C	L2
4 kW PV Array	20 mH	1.33 µF	20 mH
690 W PV Array	15 mH	0.186 µF	15 mH
560 W PV array	12 mH	2.29 µF	12 mH

4.1.2 MPPT Boost Converter

The optimum performance point can be identified as the one producing the most power. The point is called Maximum Power Point (MPP), the PV array by itself cannot regulate to operate at this point. For this reason, Maximum power point tracking (MPPT) algorithms can be developed to achieve MPP. The proposed MPPT algorithm generates a signal that is fed to the PWM generator, creating a duty signal that will control the circuit's switch. The pulsation on the switch is responsible for drawing the MPP from the PV array, increasing or decreasing the voltage. The modeled MPPT boost converter, comprised of the equivalent circuit and the control system responsible for the switching of the device is presented in Figure 24.

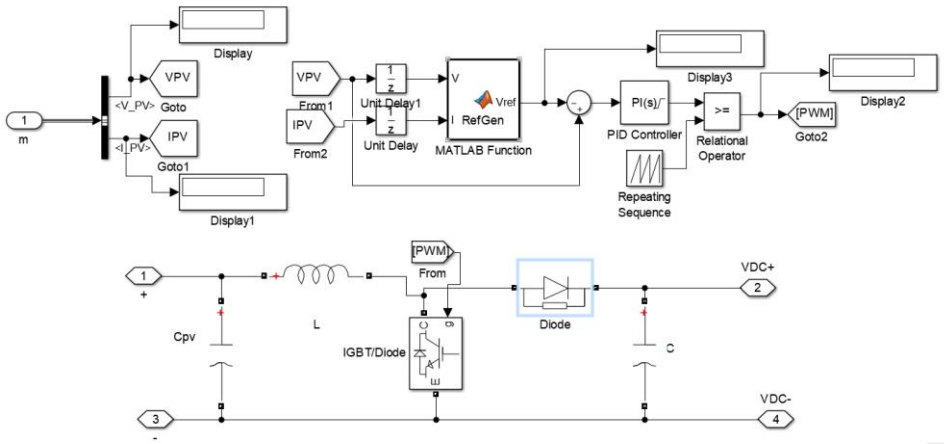

Figure 24 - Modeled 600 V DC/DC Boost Converter

Comentado [RCN17]: Not mentioned in text

The algorithm used to draw the maximum power from the PV source, in this study, is called Perturb and Observe. In this method, the MPP is reached by calculating the PV output power and the change in power by sampling the PV array voltage and current. The algorithm increments or decrements the voltage, if the perturbation leads to an increase in power, then the algorithm follows this path, if not, the algorithm perturbs in the opposite direction. A flow chart of the algorithm is presented in Figure 25. The MPPT algorithm is developed as a Matlab function block, its code is presented in the appendix, with input the current and voltage providing from the PV array, the output of the block is then the generated voltage reference (Vref). One of the disadvantages of this methodology is that some oscillation can happen between the MPP, but overall, it is a simple and effective method.

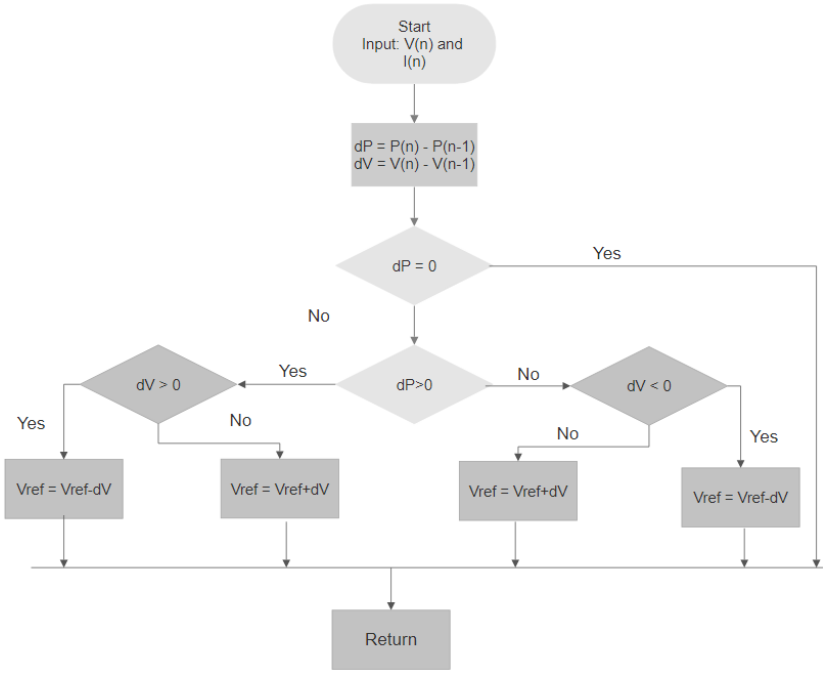

Figure 25 - Perturb and Observe flow chart

The voltage reference is then compared in a PI controller block, generating an output between 0 and 1. This output is the duty cycle fed to the PWM generator that will control the switching of the switch device integrated in the boost converter circuit drawing the MPP voltage from the PV array.

The boost converter parameters and the calculated values for inductance and output capacitance from Equation 3.19 and Equation 3.23 are:

Table 12 - DC/DC Boost Converter Parameters

	Vin	Vdc	Switch freq.	Inductance L	Capacitance C	Cpv
4 kW PV Array	230 V	600 V	5000 Hz	8 mH	1500 µF	2000 µF
690 W PV Array	75 V	600 V	5000 Hz	156 mH	186 µF	1000 µF
560W PV Array	50 V	600 V	5000 Hz	127 mH	229 µF	1000 µF

The output capacitance values selected are slightly larger to the ones calculated, the selection has been done such that the initial capacitance calculated value is used and incrementally increased until better results are observed. From a practical standpoint this methodology is not always great since a large capacitance implied a more costly circuitry. The Cpv capacitance is set such that it decreases the voltage flickers in PV generation without delaying the PV array response.

4.1.3 Control of the Two-Stage Inverter

The Two stage inverter is composed of a boost converter and an Inverter, to step the voltage to 600 V and convert the power from DC to AC 230/400 V. The control of the elements of the inverter is designed to achieve certain power conditions, such as controlling the current injected into the grid with a power factor near the unity with low harmonic distortions.

To ease the analysis and processing of the three-phase signal in the control system, Clarke and Park transformations are used to transform the three-phase signal abc into simpler direct-quadrature (dq0) and alpha-beta (αβ0) reference frames. The Clarke transformation converts three-phase abc quantities into αβ0, while the Park Transformation converts the abc quantities into dq0 quantities. The Park transformation can also be interpreted as an abc to αβ0 transformation following from a αβ0 to dq0 transformation, the relationship between the transformations is shown in Figure 26. These transformations are particularly useful for the generation of the reference signals used for the control of the inverter.

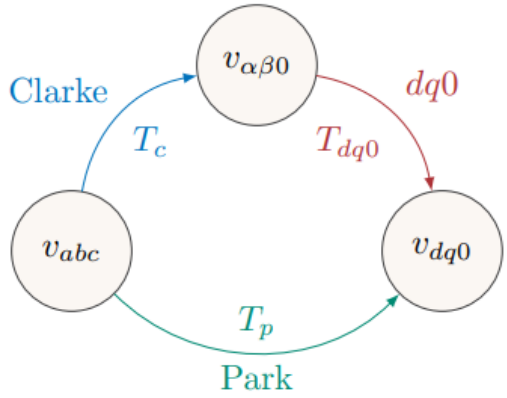

Figure 26 - Relationship between the Clarke and Park transformations taken from [34]

Comentado [RCN18]: Explain me the usefulness of this diagram

In the model, the Park transformation (abc to dq0) is done by a Simscape Power System block [35] that implements the following method, with the conventional rotating frame aligned 90 degrees behind the phase A axis:

$$\begin{pmatrix} u_d \\ u_q \\ u_0 \end{pmatrix} = \frac{2}{3} \begin{pmatrix} \sin(\omega t) & \sin\left(\omega t - \frac{2\pi}{3}\right) & \sin\left(\omega t + \frac{2\pi}{3}\right) \\ \cos(\omega t) & \cos\left(\omega t - \frac{2\pi}{3}\right) & \cos\left(\omega t + \frac{2\pi}{3}\right) \\ \frac{1}{2} & \frac{1}{2} & \frac{1}{2} \end{pmatrix} \begin{pmatrix} u_a \\ u_b \\ u_c \end{pmatrix} \quad (4.7)$$

$$V_d = \frac{2}{3}\left[V_a \sin(\omega t) + V_b \sin\left(\omega t - \frac{2\pi}{3}\right) + V_c \sin\left(\omega t + \frac{2\pi}{3}\right)\right] \quad (4.8a)$$

$$V_q = \frac{2}{3}\left[V_a \cos(\omega t) + V_b \cos\left(\omega t - \frac{2\pi}{3}\right) + \cos\left(\omega t + \frac{2\pi}{3}\right)\right] \quad (4.8b)$$

$$V_0 = \frac{1}{3}(V_a + V_b + V_c) \quad (4.8c)$$

V_a, V_b, V_c are the three phase respective voltages, V_d, V_q, V_0 are the transformed voltages in the dq0 reference frame, ω is the dq frame rotation speed and t is the time, ωt is defined as angular position of the dq rotating frame in radians (positive scalar). The inverse transformation, to obtain the dq0 to abc transformation, is given by:

$$\begin{pmatrix} u_a \\ u_b \\ u_c \end{pmatrix} = \begin{pmatrix} \sin(\omega t) & \cos(\omega t) & 1 \\ \sin\left(\omega t - \frac{2\pi}{3}\right) & \cos\left(\omega t - \frac{2\pi}{3}\right) & 1 \\ \sin\left(\omega t + \frac{2\pi}{3}\right) & \cos\left(\omega t + \frac{2\pi}{3}\right) & 1 \end{pmatrix} \begin{pmatrix} u_d \\ u_q \\ u_0 \end{pmatrix} \tag{4.9}$$

The first stage of the inverter is the Boost converter described in 4.1.2, the second stage of the inverter with decoupled control is used to convert the DC power into AC power.

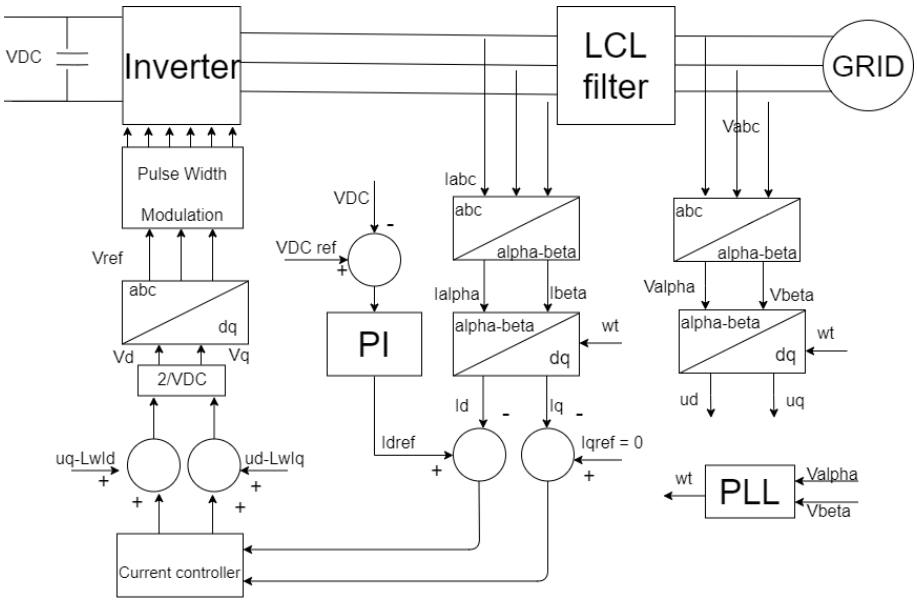

Figure 27 - Two Stage Inverter Decoupled Control Diagram

The grid-tied PV system control is composed of an inner and outer control loop. The constant DC voltage at the input of the inverter is controlled by the inner control loop, maintaining this voltage at constant level is important to maintain stability and balancing the power flow during operation.

The model uses as reference the grid's voltage and frequency for the inverter to synchronize its output and use as reference, the control system diagram is presented in Figure 27 and its Simulink model in Figure 28, and is based on the methodologies used in [36][37][38].

For the control system, the three-phase current I_{abc} is sampled at the inverter output and transformed into dq0 reference frame using Clarke and Park transformation, I_d current corresponds to the active current and I_q corresponds to the reactive current. The P and Q powers can be calculated such that

$$P = \frac{3}{2} u_d \, i_d \tag{4.10a}$$

$$Q = -\frac{3}{2} u_d \, i_q \tag{4.10b}$$

Where $u_d$and $u_q$are the respective dq axis components of the three-phase grid voltage, by controlling i_d and i_q, we are controlling the active and reactive power of the system.

The respective currents are then compared with their reference value, generating an error that is fed to the PI controller. The q axis current is forced to be 0 due to the considered simplified scenario where only active power is fed to the grid. The resulting signals is then processed in the current controller composed of individual PI controllers for each of the two signals, and generated modulation signals for the voltage in the d and q axis. The voltage drop through the filter inductor is compensated and added with the respective dq axis voltages and fed to the dq to abc block to generate the voltage reference for the PWM generator. The PWM generator duty is then to control the switches for the connection to the grid. For a Sine Wave PWM modulation scheme, the relation between modulation index and the inverter voltage is given by:

$$v_d = m_d \frac{V_{DC}}{2} \tag{4.11a}$$

$$v_q = m_q \frac{V_{DC}}{2} \tag{4.11b}$$

Decoupling the previous dynamic

$$m_d = \frac{2}{V_{DC}} [v_d - (\omega L i_q) + u_d] \tag{4.12a}$$

$$m_q = \frac{2}{V_{DC}} [v_q + (\omega L i_d) + u_q] \tag{4.12b}$$

Where $i_{dref}$and i_{qref} are the d-q axis reference currents, i_d and $i_q$are the respective dq axis components of the three-phase inverter output, $\omega L i_q$ represents the voltage drop across the filter inductor, with $\omega = 2\pi f_{grid}$ and L the value of the filter inductor.

If we define v_{td} and v_{tq}as the d-axis and q-axis components of the inverter output terminal, then the control equations can be written as

$$v_{td} = (K_p + K_i/s)(i_{dref} - i_d) - (\omega L i_q) + u_d \tag{4.13a}$$

$$v_{tq} = \left(K_p + \frac{K_i}{s}\right)(i_{qref} - q) + (\omega L i_d) + u_q \tag{4.13b}$$

Where $i_{dref}$and i_{qref} are the d-q axis reference currents, i_d and $i_q$are the respective dq axis components of the three-phase inverter output, $\omega L i_q$ represents the voltage drop across the filter inductor, with $\omega = 2\pi f_{grid}$ and L the value of the filter inductor.

In this work, only PI controllers are used to control the various steps of the method. PI controllers are used due to their simplicity of application and tuning, compared with other control methods such as PID and Fuzzy Logic for example who had an extra layer of complexity. The tuning of the controllers is achieved through the usage of the Ziegler Nichols method and predominantly manual tuning. Manual tuning of the PI controllers allows the visualization of the outputs with the change of the Proportional and Integrative parameters, giving a general direction where to increase or decrease these parameters, the tuning is complete when the controlled signals

Comentado [RCN19]: Explain me the direntce between PI controllers and PID and Fuzzy Logic.

behave like expected. The usage of this method avoids the need to define the transfer functions of the somewhat complex system but requires intuition for the tuning, which can be time consuming. The integral parameter is set to 0 at the start of the tuning similarly to the Ziegler Nichols and increase until stable condition is obtained, then the integral parameters is set to reduce the steady state error.

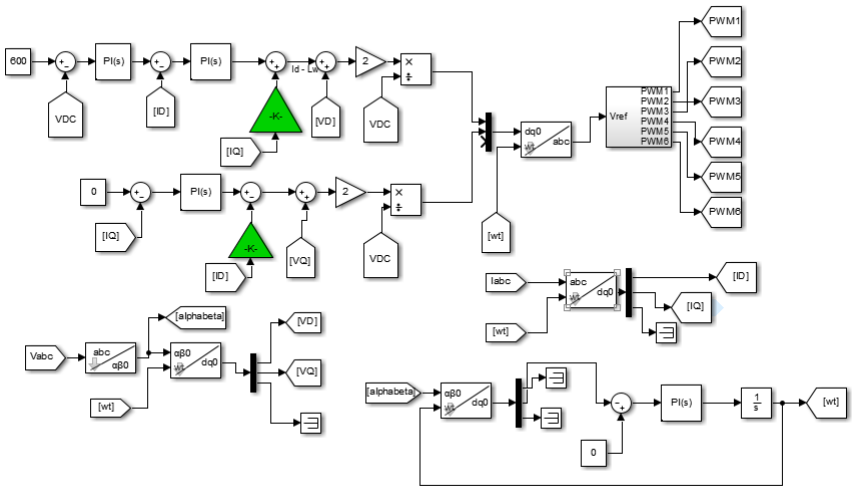

Figure 28 - Simulink Model of the Control System for the 4kW PV Array

The specifications of the model and the PI controller parameters are shown in the following, **Erro! A origem da referência não foi encontrada.** and **Erro! A origem da referência não foi encontrada.**.

Table 13 - Model system parameters

System Parameters	
Three-phase Grid Voltage, *Vg*	230/400 V AC
Grid frequency, f_{grid}	50 Hz
Rated power of PV Array, Prated	4 kW
Switching Frequency of inverter, fsw	5 kHz
DC voltage at Inverter Input	600 V

Table 14 - kp and ki parameters for the model PI controller

		4kW Array	690 W Array	560 W Array
Boost Converter DC/DC PI controller for the MPPT Algorithm	Kp	20	50	20
	Ki	0.5	0.1	0.5
DC Voltage PI Controller	Kp	5	500	100
	Ki	50	100	1
d-axis Current PI Controller	Kp	0.85	0.1	0.1
	Ki	20	0.001	0.001
q-axis Current PI Controller	Kp	100	10000	10000
	Ki	10	100	10
PLL angular position PI Controller	Kp	10	10	10
	Ki	50000	50000	50000

4.2 Model of the Battery

The battery model used for this simulation is a Li-Ion Battery with 48V Nominal Voltage, 660 Ah rated capacity. The Battery Model Parameters are calculated with Simscape Power System battery, based on the nominal properties [26]. The calculated discharge properties are presented in **Erro! A origem da referência não foi encontrada.** however the properties are assumed identical for the charging.

Table 15 - 48V 660 Ah Battery Discharge Properties

Maximum Capacity (Ah)	660
Cut-Off Voltage (V)	36
Fully Charged voltage (V)	55.8714
Nominal Discharge Current (A)	286.9565
Internal Resistance (Ω)	0.00072727
Capacity at Nominal Voltage (Ah)	596.8696
Exponential Zone Voltage (V)	51.8585
Exponential Zone Capacity (Ah)	32.4261

Another way to interpret the rated capacity of the battery, or in other words, understand how much energy is stored is done with Equation 4.14. The energy stored in the fully charged battery amounts to approximately 31.7 kWh.

$$Energy\ Stored = Rated\ capacity * Nonimal\ Voltage \quad (4.14)$$

4.2.1 Buck/Boost Converter

The Bi-directional Buck/Boost converter, Figure 29, is necessary for the microgrid mode of operation. The circuit must be able to either buck the current to a reasonable voltage for the battery so it can charge, or boost the current discharged by the battery to the AC Bus for it to meet the requirements so that the inverter is able to output the power with appropriate voltage. The DC voltage is maintained constant at the terminals of the

inverter, at 600 V. The approach, based on the methodologies of [31], for the control algorithm for the device will control the direction of the flow through a reference current generated, considering the conditions and power balance of the microgrid.

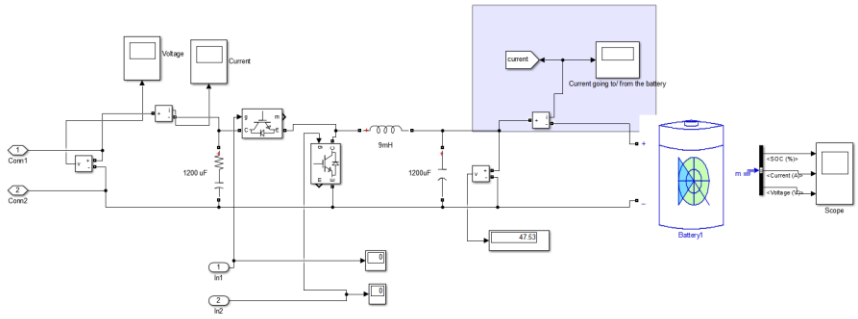

Figure 29 - Bi-Directional Buck/Boost Converter for the Battery

Comentado [RCN20]: Not mentioned in text

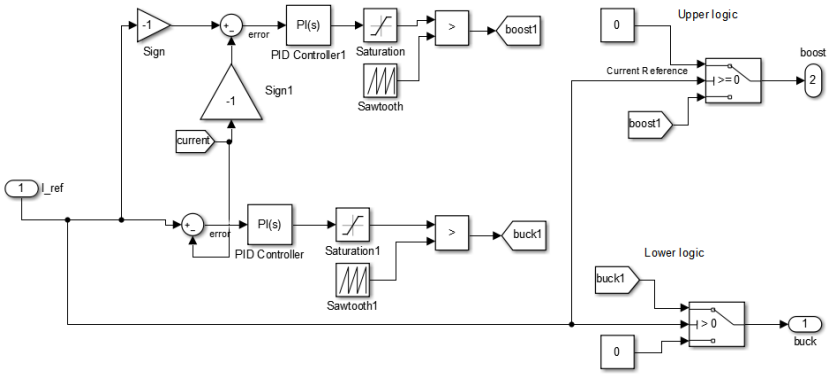

Figure 30 - Battery Control System

Comentado [RCN21]: Not mentioned in text

If the reference current I_ref is negative, the battery is discharging, then the upper logic of the control system will switch to boost mode and buck signal for the switch becomes 0, meaning it will not pulse, as presented in Figure 30. If the current is positive then the battery is in charge mode, the lower logic applies and the converter switches to buck mode and boost signal for the switch becomes 0. The buck-boost controller compares the I_ref signal with the current measured at the battery terminal, and in function of the mode of operation the signal error generated is fed to the PI controller to control the switching of the power electronic devices, through a duty cycle fed to the PWM generator.

Table 16 – Bi-directional buck/boost converter control and system parameters

Bi-Directional Buck/Boost parameters		
Inductor, L		9 mH
Capacitor Battery side		1200 µF
Capacitor Inverter Side		1200 µF
Switching Frequency for Boost/Buck		5000 Hz
Control System Parameters		
Boost PI	Kp	0.02
	Ki	3
Buck PI	Kp	0.2
	Ki	110

4.3 Microgrid

The modelled layout of the microgrid is presented in Figure 31, the three different PV sources and their respective two stage inverters, interfaced by an LCL filter, connected to the grid. The internal grid of the building is represented by the three-phase source, which allows to specify the phase-to-phase voltage, frequency and the internal impedance. The phase-to-phase voltage and frequency are chosen to be V_{pp} = 400V and 50Hz as it represents the conditions for the energy distribution in Portugal. Connected to Internal Grid a three-phase measurement unit is placed, to measure the voltage V_{abc}, the measurement is made phase-to-ground so it is expected to measure de 230V V_{rms}, the obtained results will be presented in the same way to avoid ambiguities.

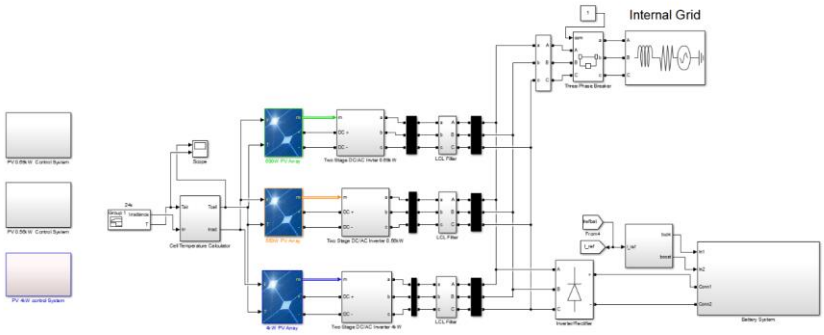

Figure 31 - Microgrid model without WECS

The ESS system is connected to the Microgrid. For small time simulations this connection works, as the charging/discharging of the battery samples in real time, so evolution of the State of Charge is observable. However, if the objective is to simulate a longer dataset, ranging from hours to years this method is not effective as the simulation will take a very long time (hours to simulate a few minutes). To be able to understand the model in full operation, instead of connecting the model to the microgrid, a separate and simpler model is constructed separately. The microgrid is run for a specified time and the variables important to simulate the State of charge, Voltage and current of the Battery are logged and synchronized in the new faster model, and then the results for the battery are obtained. This model, Figure 32, receives the logged reference battery current and with the aid of a controlled current source the battery behavior can be observed in real time.

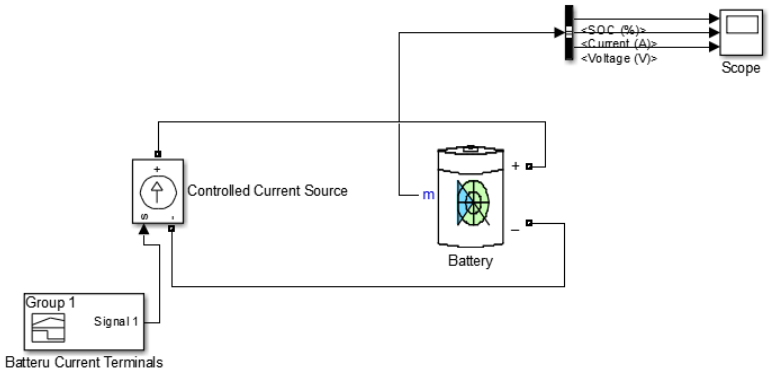

Figure 32 - Simplified model for the Battery dynamics

For example, 24 hours data are simulated in the microgrid (in 24s simulation time) and the battery current requested from the battery is logged. Then the logs are converted into a signal fed to the controlled current source which draws or feeds the battery, in the real 24 hours (86400 seconds). The battery reference signal is generated following a simple logic. Whenever the generated power is greater than the load the battery is allowed to charge, from the PV sources generation never drawing power from the internal grid, storing excess energy that due to the intermittency or mismatch with the load profile would be waste or be sold to the grid. Whenever the generated power does not meet the requirements of the load, whenever possible the battery will discharge and try to meet the load requirement. The overall objective of the model is to quantify the generation from each of the sources and measure their performance.

5 Results and Discussion

The model constructed can be of interest for the illustration of various intricacies related to the elements of the microgrid. When the interest is to observe events occurring at small time scales, the sampling time of the simulation can be several orders of magnitude decreased and the simulation time decreased to seconds. When the interest is to simulate a power balance for a month or a year, the sampling time can be adjusted, and the simulation time adjusted for the required representation of the time. This chapter focus will be on demonstrating the behavior and performance of the modeled microgrid in different time scales. The order of the results obtained, will start from smaller events (few seconds), a day, and, finally a year of simulation. The resolution of the data and sampling time for each of these simulations is adapted so that desired events are observable.

For Simulink simulations containing blocks from the Simscape Power Systems Library a Powergui block is necessary to store the equivalent Simulink circuit that represent the state-space equations of the model. The block allows to choose the solving of the equations of the model to be in continuous or discrete, at fixed or variable step. The chosen solving method used is Discrete, which performs a discretization of the model using a specified sample time. The sample time is chosen to be in the order of 10^{-5} s so that events happening at the switching frequency from the converters are observable without slowing the simulation time excessively. The solver is also configured to use a variable step-time so that whenever the outputs of the equations are in steady-state the step time increases to speed up simulation time.

5.1 MPPT Algorithm performance

The evaluation of the performance of MPPT algorithm is done through measuring the voltage and current generated by the PV with MPPT and obtain the power curve. For comparison an ideal curve is generated based on the maximum power obtained at STC. The efficiency of the MPPT is then evaluated with the equation 5.1 with the power generated from PV array being calculated with Equation 3.4, the Simulink blocks are displayed in.

$$\eta_{mppt-} = 1 - \frac{\left|P_{pv-}P_{ideal}\right|}{P_{ideal}} \tag{5.1}$$

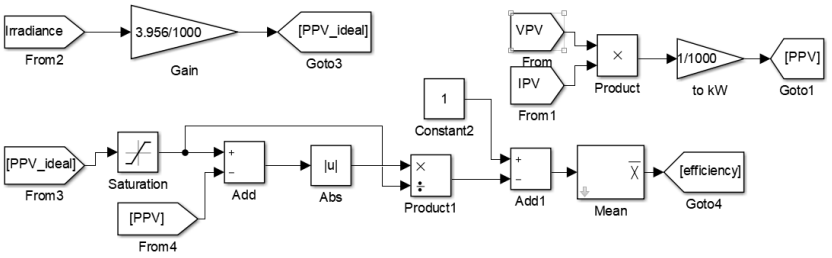

Figure 33 - Simulink blocks to evaluate MPPT efficiency

The efficiency of the MPPT algorithm for the three modeled PV array are shown in Figure 34, 35 and 36. The obtained Power extracted from the PV Array is close to the maximum available power, hence the MPPT algorithm works as expected. The mean efficiency of the MPPT algorithm is close to unity when the system is in steady state. The irradiance used to evaluate the performance, displays a stair like curve, starting from 200 W/m^2 then jumping to 400 W/m^2, 600 W/m^2, 1000 W/m^2 and back to 600 W/m^2, over 11 seconds.

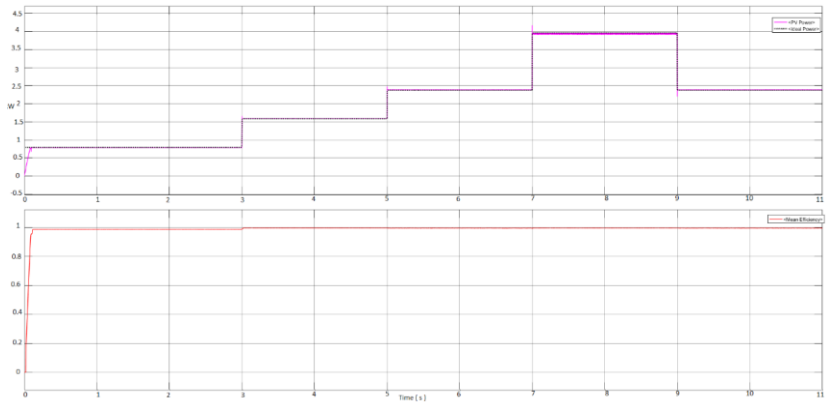

Figure 34 - Extracted power from 4 kW PV Array and MPPT efficiency

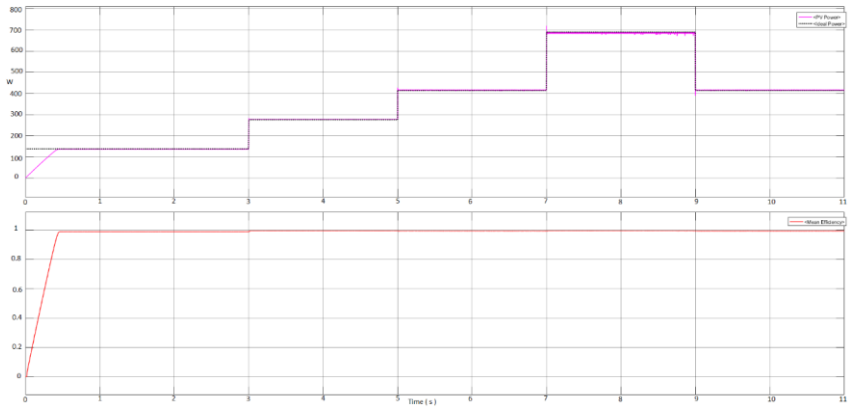

Figure 35 - Extracted power from 690 W PV Array and MPPT efficiency

Comentado [RCN22]: Not mentioned in text

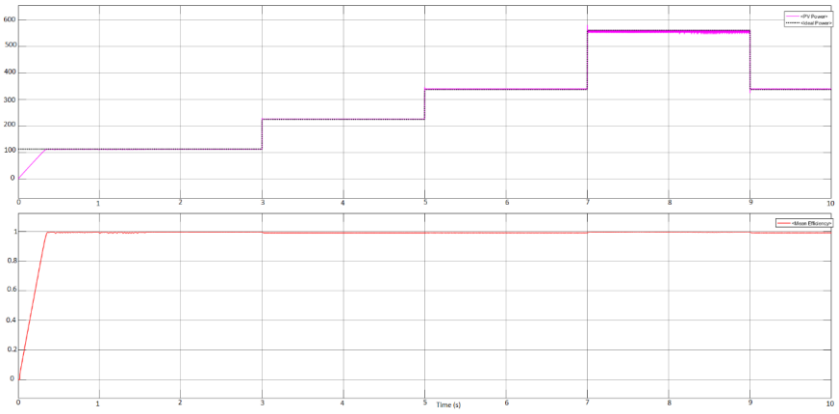

Figure 36 - Extracted power from 560 W PV Array and MPPT efficiency

Comentado [RCN23]: Not mentioned in text

5.2 Photovoltaic Array generation

The microgrid model is run for 1 second at STC conditions (1000 W/m^2, T=25 °C) to observe the various output that represent the operation of the system in terms of power generation. The three-phase voltage and current at output of the inverter, the PV output current and voltage, and the DC voltage at the input of the DC/AC converter. The chosen V_{dc} = 600 V, is important to guarantee that the inverter input voltage is sufficient to generate the output voltages (Vabc) at 230/400 V. As seen in the Figure 37 the peak voltage for each phase of V_{abc} is 325 V, which indicates that inverter control manages to convert the voltage appropriately. The peak voltage of V_{abc} is calculated with Equation 5.2, which corroborates with the theory that the phase-to-neutral 230 V is the root mean square voltages and the 400V is phase-to-phase voltage.

$$Vphase\_ground_{peak} = \sqrt{2} * 230 = 325\ V \tag{5.2}$$

The currents however are slightly more complicated to control and this is shown in the results. Unlike the voltages that used as reference the grid, the current reference is created through a control loop, which generated some distortion, as shown in Figure 37. In the decoupling control algorithm, the three-phase current and voltages are transformed into the dq reference frame, the direct current (I_d) reference is generated through the inner control loop, however the quadrature current reference (I_q) is set to 0 as the scenario imposed to the microgrid where there is no reactive power required from the inverters. The three-phase current and voltages are in phase which indicates the power factor is close to the unity and that the inverters are feeding the AC bus with active power. The AC bus voltage and current injected are shown in Figure 38, the current peaking at $Iabc_{Peak} = 12.6\ A$.

Comentado [RCN24]: Do the legend of the different colors lines

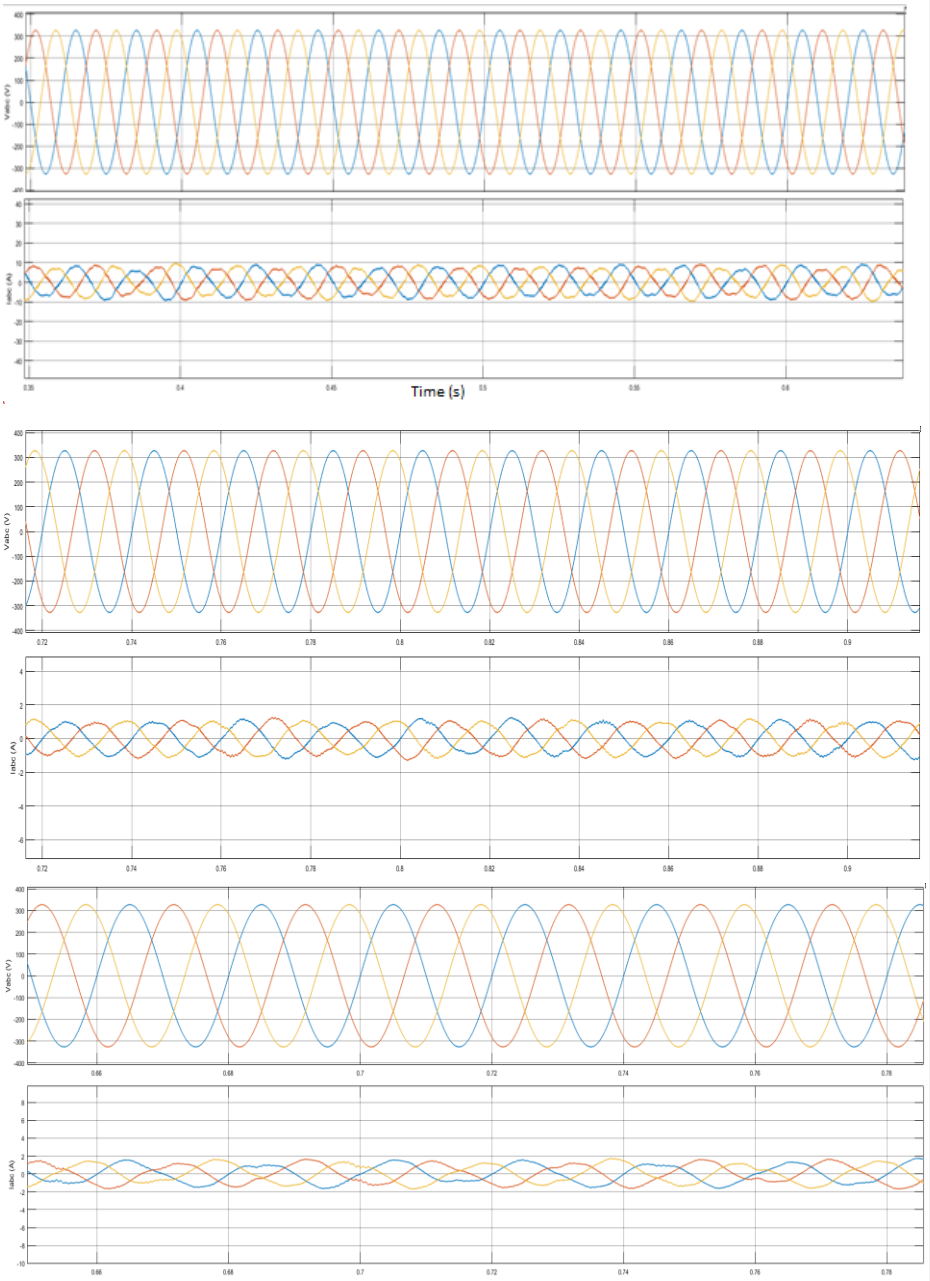

Figure 37- Vabc and Iabc at the inverter output for the 4 kW PV array (top), 690 W PV array (middle) and 560W PV panels (bottom). With each of the colored line representing the voltage and the current of the three-phases, Red – Va and Ia, Yellow – Vb and Ib, and Blue – Vc and Ic.

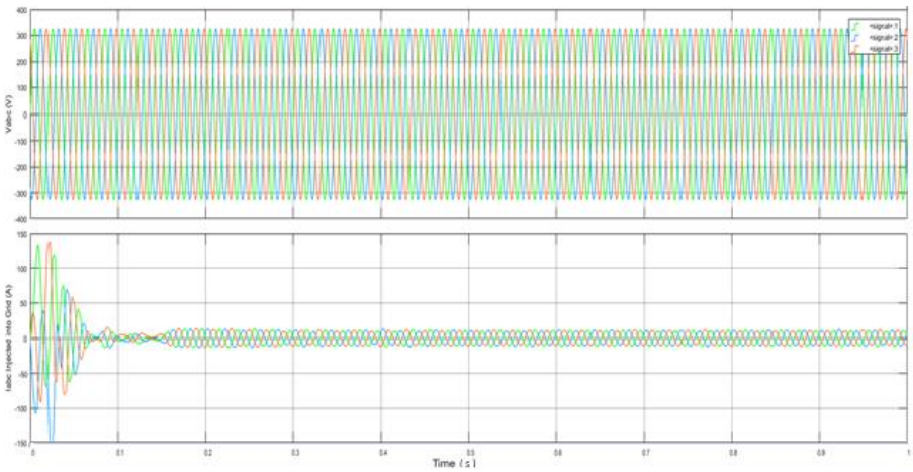

Figure 38 - Vabc and Iabc measured in Microgrid AC Bus

The maximum power fed to microgrid from the PV sources can be then calculated using the following equation

$$P = \sqrt{3} * V * I * pf \quad (5.3)$$

Where V=230V, I = 12.6 A and the power factor (pf) is considered to be 0.95 due to the reactive power induced by the switching devices of the inverter, for STC conditions the maximum power injected into the grid is calculated P_{ACbus}= 4.768 kW. The value obtained previously can then be compared with the sum of the power generated at the terminals of the PV arrays, Figure 39. This comparison can provide an approximation of the losses obtained in the circuitry between the terminals of the PV array and the AC bus, namely the losses in the converters.

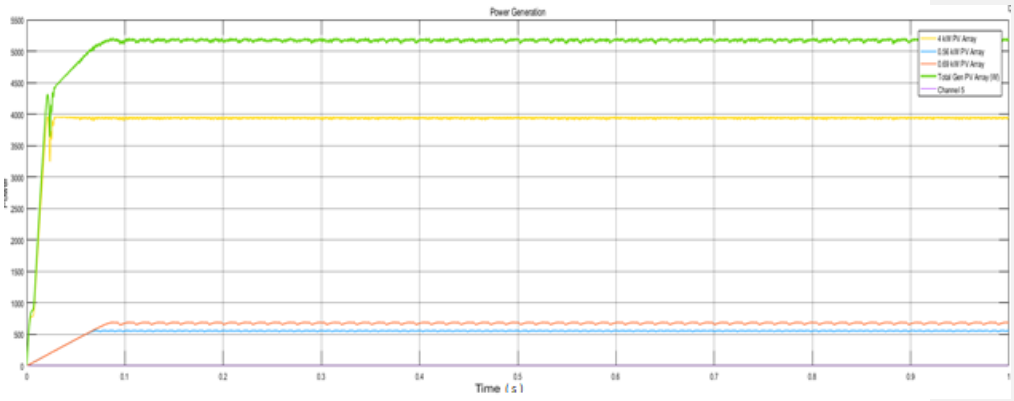

Figure 39 - Power generation calculated at the terminals of the PV array

The mean power generation in the STC for the PV Arrays before the converters is $P_{source} = 5174\ W$, the losses that interface the generation and the AC bus are estimated as

$$Losses_{interface} = P_{source} - P_{ACbus} \quad (5.4)$$

And a global efficiency for the conversion process can be expressed as the ratio between the power generated and power injected into the bus.

$$\eta_{globalconversion} = \frac{P_{ACbus}}{P_{source}} \quad (5.5)$$

Obtaining a global conversion efficiency $\eta_{globalconversion}$ 94% amounting the losses to 406 W.

For comparison term, the maximum efficiency of a commercial inverter with MPPT like the SMA Sunny boy amounts to around 97% [39]. The methodology used to estimate the efficiency of the converters is not the most precise and should not be considered for exact calculations but gives a rough idea of the power losses due to the converter's switches.

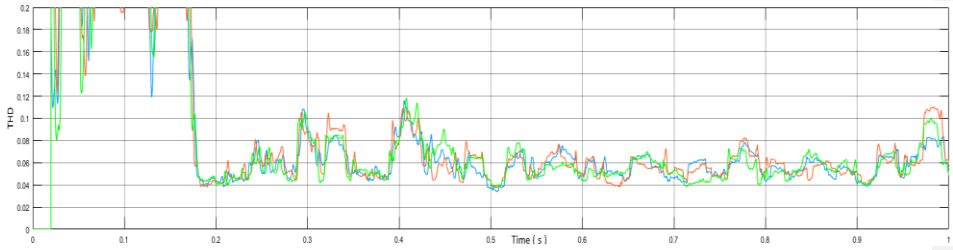

Figure 40 - Total Harmonic Distortion for each phase of the AC Bus Current

The IEEE determines that the current distortion limits for general distribution systems (starting from 120V) the maximum harmonic current distortion should be lower than 5% for systems whose bus voltage is inferior to 69kV, as such to avoid feeding power without quality which can damage equipment or when in grid-tied disturb the normal operation of the grid. [40].

Comentado [RCN25]: Explain me on that

The resulting current flowing in the AC bus THD levels are shown in Figure 40, the overall quality of the current is poor as the THD levels are above the maximum levels for operation of power systems. The cause for the signal flicker and distortion is related to the conversion system and its control of the current. Further work is required to optimize the controller and troubleshoot to obtain a better signal.

In Figure 38 large and fast spikes are observed, they exist because at the start of the simulation the voltage across the terminals of the generators is zero, and thus no current is flowing, however the grid perceives the connecting capacitor at the inverter output as a load and charges it quickly, creating the burst observed at start of the simulation, but the inverter control stabilizes the capacitor terminal voltages rapidly as illustrated in Figure 41.

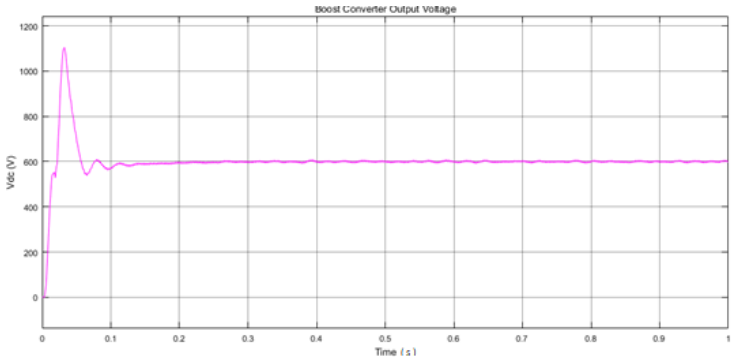

Figure 41 - DC voltage at Inverter Input

5.3 Daily Simulation

To run the daily simulation, an Irradiance and Temperature dataset is taken from the SolTerm 6 software, the data file presents the hourly averaged values for the whole year of 2016. The software outputs the data as csv. File that is then converted into .xls file to ease the reading and manipulation of the data. The daily simulation is done for a characteristic day of each of the four seasons.

A load profile has been sketched, Figure 42, to represent the dynamic of loads and the generation. A base 1 kW through the day is assumed to feed laboratory equipment that must remain turned ON, between 8h to 19h the place is considered to be populated increasing the consumption required for computers and lighting and other small appliances. Between 10h and 12h (peak) and 14h to 19h the consumption levels are at their highest, justified by increased load on the heat pump for domestic hot water and air conditioning of the spaces.

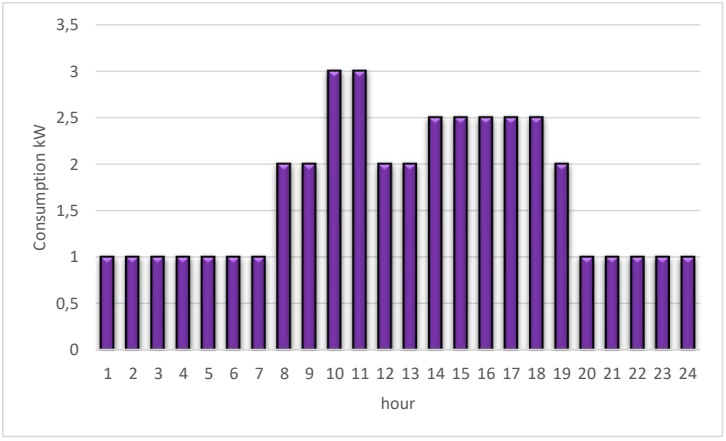

Figure 42 - Load profile for the considered zone

Comentado [RCN26]: Not mentioned in text

For the simulation, the initial State of charge (%SOC) of the battery is considered to be 50%, and will discharge to the AC bus whenever the generation doesn't meet the load requirements and will charge accordingly whenever the generation is sufficient for the load. No partial shading effects are simulated, and the temperature of the solar cell is modelled according to equation 4.1.

Table 17- Summer Simulation Parameters

Simulation Parameters	
Sampling time	5e-05 s
Initial %SOC Battery	50%
Simulation time	1 day (condensed into 24s of simulation)
Irradiance and Temperature Data	10 August 2016

The hourly averaged values for the Irradiance (W/m^2) and Temperature (°C) are displayed in Figure 43. The generated power for each of the DER sources is presented in Figure 43, each colored line for each generator, the green line is the sum of each of the individual power generated at a certain time.

$$P_{PV_{TOTAL}}(t) = P_{PV1}(t) + P_{PV2}(t) + P_{PV3}(t) \quad (5.6)$$

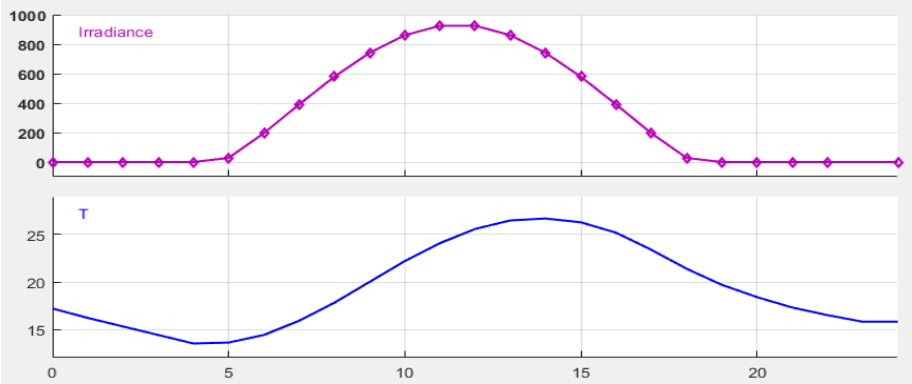

Figure 43 - Irradiance and Temperature Curve for the summer simulation

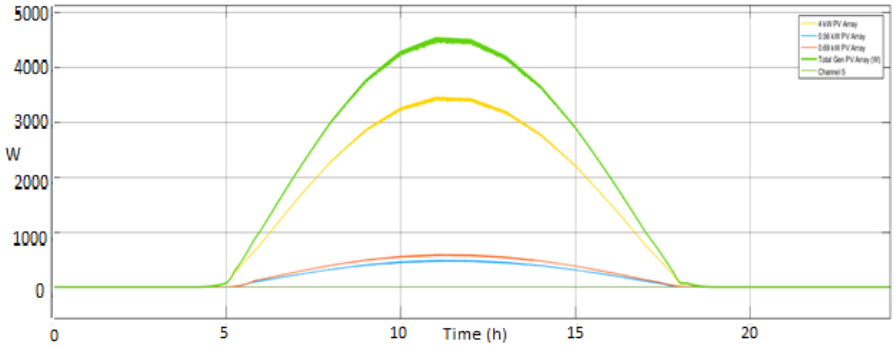

Figure 43 - PV generation by source and total PV Generation for the summer simulation

For the summer time the load profile and the PV generation curve "fit", as seen in Figure 44. The peak load and peak generation coincide, and allowing battery charging during daytime.

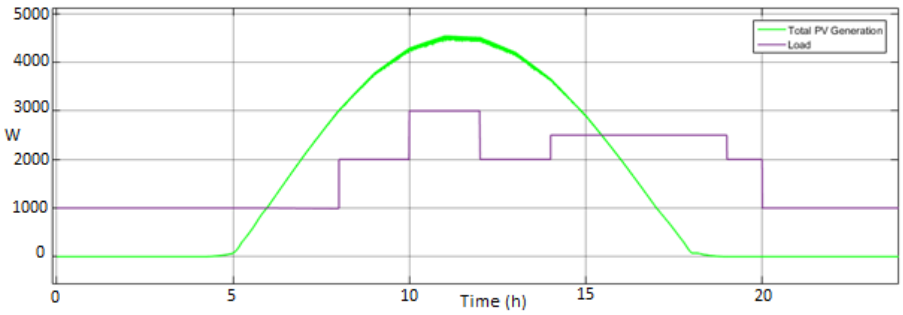

Figure 44 - "Fitting" of the Generation and load for the summer simulation

To understand whether there is need to draw power or feed the battery or grid, the Equation 5.7, evaluates the generation and the load. If the value is positive the generation is larger than the load, and the battery switches to charge mode, if full the power is fed to the grid. In the case of a negative value the battery switches to discharge mode and feeds the load until no charge is available, the grid must then feed load.

$$P_{Balance}(t) = P_{Generation}(t) - P_{Load}(t) \quad (5.7)$$

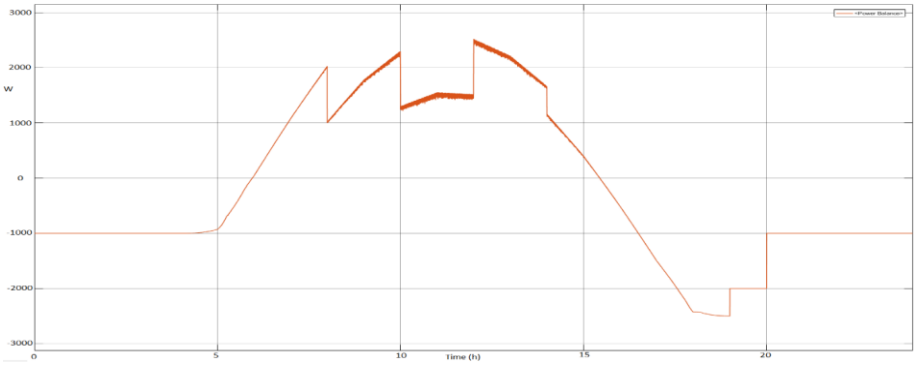

Figure 45 - Calculated Power Balance for the summer simulation

Comentado [RCN27]: Not mentioned in text

In Figure 46, the dynamic of the charging and discharging of the battery and the battery current are shown. For the scenario, the battery handles the periods where the load is greater than the generation and has the conditions to charge even when the load is peaking.

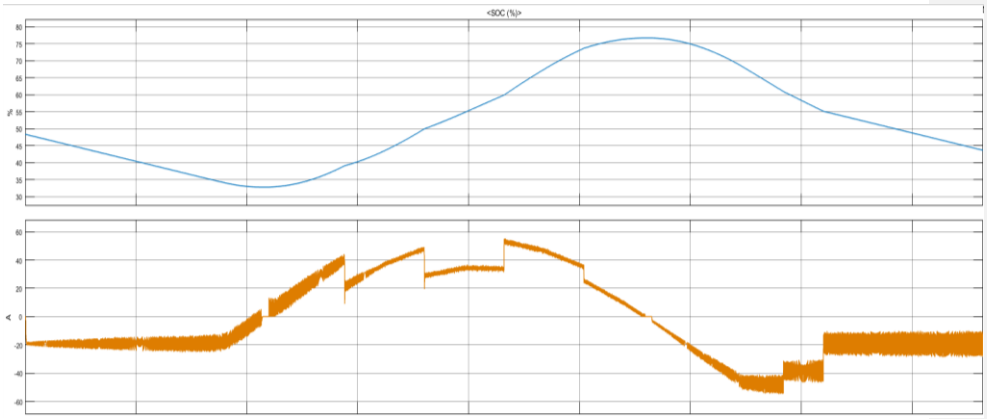

Figure 46 - State of Charge of the Battery along the 24h of simulation and the battery current for the summer simulation

5.4 Annual Simulation

The dataset to perform the annual simulation is comprised of 8761 values for the air temperature and irradiance in Lisbon, each corresponding to the average value for the hour of the year of 2016 as seen in Figure 47. The load profile for the simulation is considered constant throughout the year, and the same that used in Section 5.3.

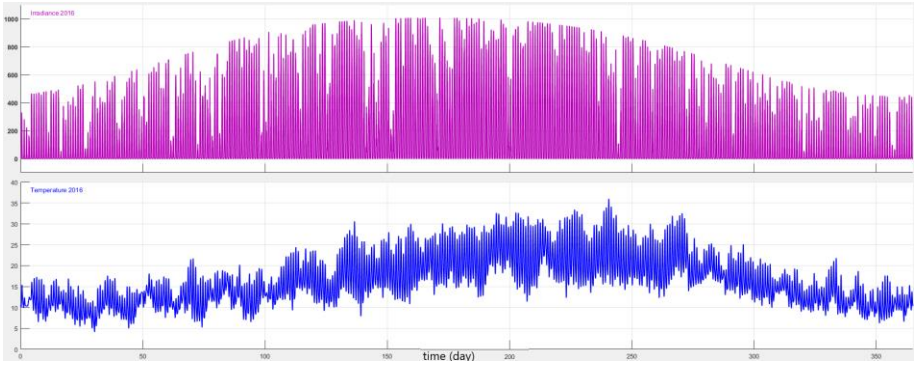

Figure 47 - Temperature and Irradiance values (Lisbon, 2016) extracted from SolTherm5

The daily PV generation for the full year can be inspected in Figure 49. Figure 50 purpose is to inspect if the sample time used for the year simulation is adequate to give the intended results, the scope is zoomed to

capture the information for different days.

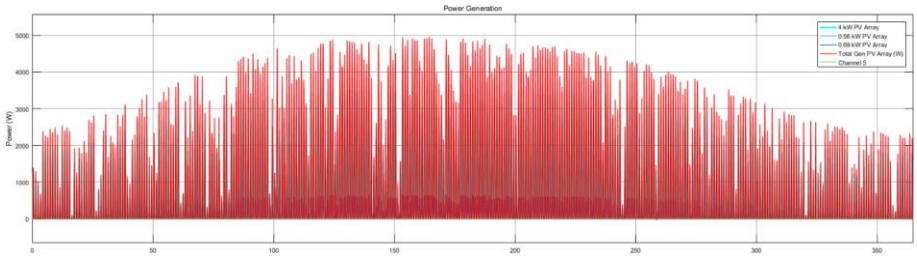

Figure 48 - Microgrid photovoltaic Generation for 2016 data

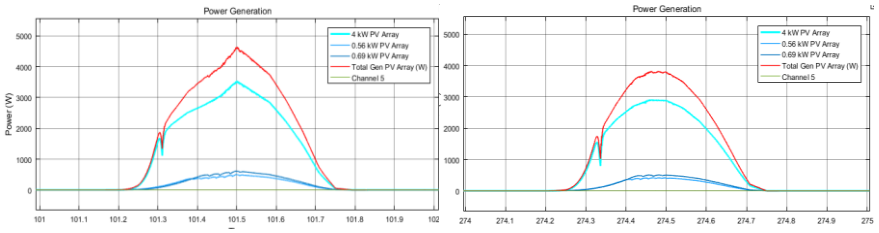

Figure 49 - Selected two days of the year for inspection of the daily data for the annual simulation

Comentado [RCN28]: What do you want to compare with this two days?

Comentado [RCN29]: This figure is not in the figures index

The resolution and the sampling period yield satisfactory results that can prove to be useful for the estimation of the energy balance for the year. The days zoomed are chosen randomly so to illustrate the resolution of the daily results for the whole simulation, being sufficient for the estimation of the mean daily generation.

The obtained mean photovoltaic generation for the simulation, is presented in Table 18.

Table 18 - Mean Annual Generation and Load

Source	Annual Mean Power (kW)	Mean annual Energy Generated (kWh)
PV1 – 4kW Rated	0.689	6035.6
PV2 – 0.69 kW Rated	0.101	884.8
PV3 – 0.56 kW Rated	0.088	770.9
Total Generation	0.878	7690.8
Load	2.09	18308.4
Power Balance	-	-10617.6

The average mean power, like previously indicated that the PV generation is not sufficient to feed constant loads like the load profile considered. For this reason, like previously mentioned in the thesis, ESS and generators that can operate with a lesser time constraint (not only the day) greatly complement the integration of photovoltaic systems in microgrids. From the balance developed we can conclude that 42% of the electricity consumption of the building is produced by the photovoltaic source. The 58% need to be provided from the battery, the WECS or the grid. However, this percentages represent an estimation, since the dynamic is not linear, most of the PV generation occur when the load is at its peak.

6 Conclusion

The work performed in the thesis allowed to model three of the power generators presented in the microgrid and design their converting control system. Due to inexperience in the handling of the simulation software a mistake has been made where the time scale of the generation is not equal to the time scale ESS, making an analysis of the battery dynamics complicated. However, the issue was fixed by logging the data from the output of the Microgrid generation side and inputting it in a separate simulation for the ESS.

Due to the pandemic and internal events in the LNEG there was a noticeable lack of communication between the responsible for the project and the coordination of the thesis, leading to many assumptions that may not be in concordance with the reality and the model of Wind Turbine not being included for the generation.

Further work includes creating a model for the WECS and integrate it with the electrical system and thermal system, adapt the model to be able to detect fault conditions and be able to switch to Island Mode within the power quality conditions. Create an intelligent microgrid management system with the capability to determine whenever the excess power should be sold to the grid or be stored in ESS, through economic analysis and predictive control.

The thesis came as a great challenge, speaking from experience, mechanical engineering students are not familiar with most technicalities and theory related to electricity and the power systems. However, the development of the thesis had a great impact over my knowledge about many faces of the power generation that were not considered previously when looking at power systems.

Comentado [RCN30]: What type of gains can we get from this efficient controls of microgrids?

Comentado [RCN31]: What had you done different if you star the thesis right now with the current knowledge?

REFERENCES

Comentado [RCN32]: The references are in Harvard style. The should be in the style IEEE 2006

[1] "Portugal - Countries & Regions - IEA," *IEA World Energy Balances 2020*. [Online]. Available: https://www.iea.org/countries/portugal. [Accessed: 17-Jan-2021].

[2] H. Zhao, H. Zhao, S. Guo, F. Li, and Y. Hu, "The impact of financial crisis on electricity demand: A case study of North China," *Energies*, vol. 9, no. 4, pp. 1–13, 2016.

[3] G. de Portugal, "Plano Nacional Energia E Clima 2021-2030," vol. 2030, no. Pnec 2030, 2019.

[4] R. H. Lasseter, "MicroGrids: A Conceptual Solution," *2002 IEEE Power Eng. Soc. Winter Meet. Conf. Proc. (Cat. No.02CH37309)*, vol. 1, pp. 305–308, 2002.

[5] E. Hossain, E. Kabalci, R. Bayindir, and R. Perez, "Microgrid testbeds around the world: State of art," *Energy Convers. Manag.*, vol. 86, pp. 132–153, 2014.

[6] "Types of Microgrids | Building Microgrid." [Online]. Available: https://building-microgrid.lbl.gov/types-microgrids. [Accessed: 04-May-2020].

[7] "Isle of Eigg | Building Microgrid." [Online]. Available: https://building-microgrid.lbl.gov/isle-eigg. [Accessed: 04-May-2020].

[8] M. A. Hossain, H. R. Pota, M. J. Hossain, and F. Blaabjerg, "Evolution of microgrids with converter-interfaced generations: Challenges and opportunities," *Int. J. Electr. Power Energy Syst.*, vol. 109, no. December 2018, pp. 160–186, 2019.

[9] A. T. Elsayed, A. A. Mohamed, and O. A. Mohammed, "DC microgrids and distribution systems: An overview," *Electr. Power Syst. Res.*, vol. 119, pp. 407–417, 2015.

[10] S. Parhizi, H. Lotfi, A. Khodaei, and S. Bahramirad, "State of the art in research on microgrids: A review," *IEEE Access*, vol. 3, pp. 890–925, 2015.

[11] H. Daneshi and H. Khorashadi-Zadeh, "Microgrid energy management system: A study of reliability and economic issues," *IEEE Power Energy Soc. Gen. Meet.*, pp. 1–5, 2012.

[12] A. Khodaei, "Resiliency-oriented microgrid optimal scheduling," *IEEE Trans. Smart Grid*, vol. 5, no. 4, pp. 1584–1591, 2014.

[13] A. Vinayagam, K. Swarna, S. Y. Khoo, and A. Stojcevski, "Power Quality Analysis in Microgrid: An Experimental Approach," *J. Power Energy Eng.*, vol. 04, no. 04, pp. 17–34, 2016.

[14] A. Vinayagam, A. Aziz, K. S. V. Swarna, S. Khoo, and A. Stojcevski, "Power Quality Impacts in a Typical Microgrid," no. Seee, pp. 77–82, 2015.

[15] T. S. Ustun, C. Ozansoy, and A. Zayegh, "Recent developments in microgrids and example cases around the world - A review," *Renew. Sustain. Energy Rev.*, vol. 15, no. 8, pp. 4030–4041, 2011.

[16] "CERTS Microgrid Test Bed | CERTS." [Online]. Available: https://certs.lbl.gov/initiatives/certs-microgrid-test-bed. [Accessed: 15-May-2020].

[17] A. A. Renjit, M. S. Illindala, R. H. Lasseter, M. J. Erickson, and D. Klapp, "Modeling and control of a natural gas generator set in the CERTS microgrid," *2013 IEEE Energy Convers. Congr. Expo. ECCE 2013*, pp. 1640–1646, 2013.

[18] R. H. Lasseter *et al.*, "CERTS microgrid laboratory test bed," *IEEE Trans. Power Deliv.*, vol. 26, no. 1, pp. 325–332, 2011.

[19] H. Tsai, C. Tu, and Y. Su, "Development of Generalized Photovoltaic Model Using MATLAB/SIMULINK," *Lect. Notes Eng. Comput. Sci.*, vol. 2173, no. 1, pp. 846–851, 2008.

[20] R. Ben Ali, H. Schulte, and A. Mami, “Modeling and simulation of a small wind turbine system based on PMSG generator,” *IEEE Conf. Evol. Adapt. Intell. Syst.*, vol. 2017-May, no. October, 2017.

[21] Y. H. Han, "Wind Energy Conversion Systems" in *Grid Integration of Wind Energy Conversion Systems*, vol. 21, no. 3–4. 2000.

[22] “Implement model of variable pitch wind turbine - Simulink.” [Online]. Available: https://www.mathworks.com/help/physmod/sps/powersys/ref/windturbine.html. [Accessed: 12-Oct-2020].

[23] N. Phankong, S. Manmai, K. Bhumkittipich, and P. Nakawiwat, “Modeling of grid-connected with permanent magnet synchronous generator (PMSG) using voltage vector control,” *Energy Procedia*, vol. 34, pp. 262–272, 2013.

[24] “Three-phase permanent magnet synchronous machine with sinusoidal or trapezoidal back electromotive force, or five-phase permanent magnet synchronous machine with sinusoidal back electromotive force - Simulink.” [Online]. Available: https://www.mathworks.com/help/physmod/sps/powersys/ref/permanentmagnetsynchronousmachine.html. [Accessed: 01-Nov-2020].

[25] P. Gregory, "Battery Boot Camp" in *Battery Modelling - Battery Management Systems*, vol. 1, no. 1. 2015.

[26] “Generic battery model - Simulink.” [Online]. Available: https://www.mathworks.com/help/physmod/sps/powersys/ref/battery.html. [Accessed: 12-Dec-2020].

[27] N. Muhammad H. Rashid Kumar and A. R. (Ashish R. Kulkarni, *Power electronics : devices, circuits and applications*. 2014.

[28] B. Hauke, “Basic Calculation of a Boost Converter’s Power Stage,” *Texas Instruments, Appl. Rep. Novemb.*, no. November 2009, pp. 1–9, 2009.

[29] F. Mohammed Al-Raie and H. Qasim, “Design And Implementation Of A Microcontroller Based DC/AC Inverter” *Al Mansour Journal*, no. December 2015, p. 19, 2015.

[30] N. T. D. Fernandes *et al.*, “Control strategy for pulsed lead acid battery charger for stand alone photovoltaics,” *2015 IEEE 13th Brazilian Power Electron. Conf. 1st South. Power Electron. Conf. COBEP/SPEC 2016*, no. November, 2015.

[31] M. Saleh, Y. Esa, Y. Mhandi, W. Brandauer, and A. Mohamed, “Design and implementation of CCNY DC microgrid testbed,” *IEEE Ind. Appl. Soc. 52nd Annu. Meet. IAS 2016*, pp. 1–7, 2016.

[32] R. Ayaz, I. Nakir, and M. Tanrioven, “An improved matlab-simulink model of pv module considering ambient conditions,” *Int. J. Photoenergy*, vol. 2014, 2014.

[33] M. Dursun and M. K. Dosoglu, “LCL Filter Design for Grid Connected Three-Phase Inverter,” *ISMSIT 2018 - 2nd Int. Symp. Multidiscip. Stud. Innov. Technol. Proc.*, no. June, pp. 2–6, 2018.

[34] C. J. O’Rourke, M. M. Qasim, M. R. Overlin, and J. L. Kirtley, “A Geometric Interpretation of Reference Frames and Transformations: Dq0, Clarke, and Park,” *IEEE Trans. Energy Convers.*, vol. 34, no. 4, pp. 2070–2083, 2019.

[35] MATLAB, “Perform transformation from αβ0 stationary reference frame to dq0 rotating reference frame or the inverse - Simulink,” *Matlab2007*, 2007. [Online]. Available: https://www.mathworks.com/help/physmod/sps/powersys/ref/alphabetazerotodq0dq0toalphabetazero.html. [Accessed: 25-Dec-2020].

[36] M. Lakshmi and S. Hemamalini, “Decoupled control of grid connected photovoltaic system using fractional order controller,” *Ain Shams Eng. J.*, vol. 9, no. 4, pp. 927–937, 2018.

[37] P. K. Khatua, V. K. Ramachandaramurthy, J. Y. Yong, and J. Pasupuleti, “Decoupled Control of Three Phase Grid Connected Solar PV System,” *Int. J. Eng. Adv. Technol.*, vol. 9, no. 2, pp. 4218–4222, 2019.

[38] P. K. Pathak, A. Kumar Yadav, and P. Tyagi, “Design of Three Phase Grid Tied Solar Photovoltaic System Based on Three Phase VSI,” *India Int. Conf. Power Electron. IICPE*, vol. 2018-Decem, 2018.

[39] S. M. A. Solar and T. Ag, “Integrated service for ease and comfort,” [Online]. Available: https://www.sma.de/en/products/solarinverters/sunny-boy-30-36-40-50-60.html. [Accessed: 29-DEC-2020]

[40] “IEEE Recommended Practices and Requirements for Harmonic Control in Electric Power Systems, “IEEE std 519-1992,” *Ieee*, pp. 1–9, 1992.

APPENDICES

Appendix A

Perturb and Observe algorithm for MPPT Calculation

```
function Vref = RefGen(V,I)

%Algoritmo P&O

Vrefmax = 330;
Vrefmin = 0;
Vrefinit = 200;
deltaVref =0.5;
persistent Vold Pold Vrefold

datatype = 'double';
if isempty(Vold)
    Vold = 0;
    Pold = 0;
    Vrefold = Vrefinit;
end

P = V*I;
dV = V-Vold;
dP = P-Pold;

if dP ~= 0
    if dP<0
        if dV<0
            Vref = Vrefold + deltaVref;
        else
            Vref = Vrefold-deltaVref;
        end
    else
        if dV<0
            Vref=Vrefold-deltaVref;
        else
            Vref = Vrefold+deltaVref;
        end
    end
else Vref = Vrefold;
end
if Vref >= Vrefmax | Vref <= Vrefmin
    Vref = Vrefold;
end
Vrefold = Vref;
Vold = V;
Pold = P;
```

Appendix B

Matlab Code for the Irradiance and Temperature curve generation

```
Irradiance = [dataset]
step = 24/length(irradiance) %time/length
a = 0;
for i = 1:length(irradiance)
    timewinter(i)=a;
    a=a+step;
end
plot(timewinter,irradiance);
plot(timewinter,temperature);
```

Appendix C

Simulink Model of the Microgrid

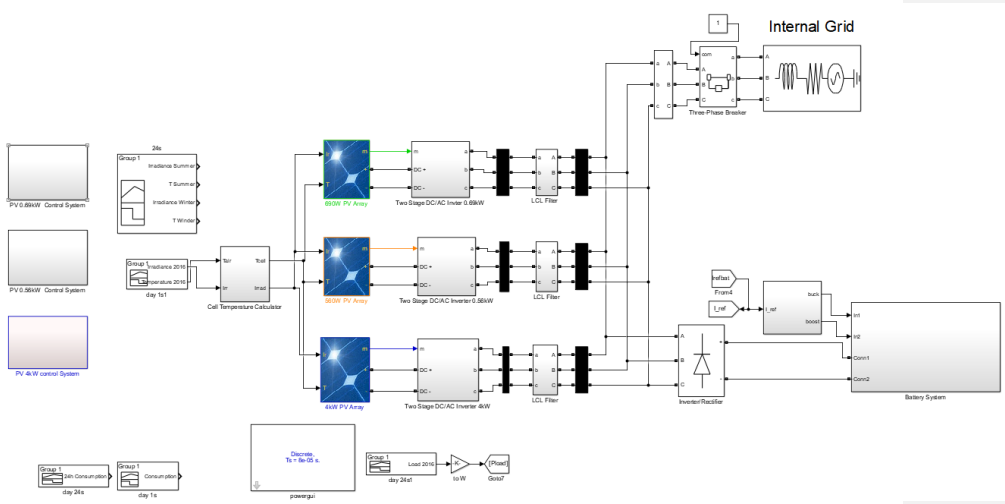

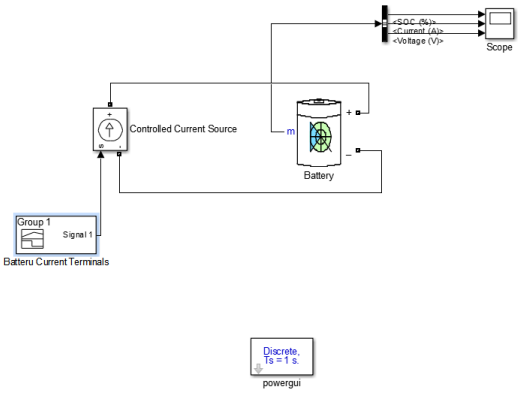
<SOC (%)>
<Current (A)>
<Voltage (V)>
Scope
Controlled Current Source
m
+
–
Battery
Group 1
Signal 1
Batteru Current Terminals
Discrete,
Ts = 1 s.
powergui